Patterns in randomly evolving networks: Idiotypic networks

Markus Brede and Ulrich Behn

Institut für Theoretische Physik, Universität Leipzig, Augustusplatz 10, D-04109 Leipzig, Germany
(Received 16 August 2002; published 31 March 2003)

We present a model for the evolution of networks of occupied sites on undirected regular graphs. At every iteration step in a parallel update, I randomly chosen empty sites are occupied and occupied sites having occupied neighbor degree outside of a given interval (t_1, t_u) are set empty. Depending on the influx I and the values of both lower threshold and upper threshold of the occupied neighbor degree, different kinds of behavior can be observed. In certain regimes stable long-living patterns appear. We distinguish two types of patterns: static patterns arising on graphs with low connectivity and dynamic patterns found on high connectivity graphs. Increasing I patterns become unstable and transitions between almost stable patterns, interrupted by disordered phases, occur. For still larger I the lifetime of occupied sites becomes very small and network structures are dominated by randomness. We develop methods to analyze the nature and dynamics of these network patterns, give a statistical description of defects and fluctuations around them, and elucidate the transitions between different patterns. Results and methods presented can be applied to a variety of problems in different fields and a broad class of graphs. Aiming chiefly at the modeling of functional networks of interacting antibodies and B cells of the immune system (idiotypic networks), we focus on a class of graphs constructed by bit chains. The biological relevance of the patterns and possible operational modes of idiotypic networks are discussed.

I. INTRODUCTION

Many complex coupled systems can be modeled as networks: Vertices being associated with the systems' elements and edges representing interactions between them. Metabolic networks [1,2], food webs [3], social networks [4], and networks in the immune system (for some approaches see Ref. [5]) are some examples of such systems. Frequently, although the detailed interactions of the elements may be rather complicated, the knowledge of the underlying network structure facilitates the understanding of essential features of the system as a whole [6].

In the absence of detailed knowledge of a network's topology, previous works tended to assume either a completely random link structure [7–9] or clusters given by percolation on lattices [10]. The complexity of many systems, however, emerges as a consequence of some underlying principle for their evolution, e.g., preferential attachment [11], optimization of transportation and communication pathways [12–14], extinction of the least populated species [15,16], or of the mere fact that the network has randomly evolved in time [17]. This altogether may lead to a highly organized network topology.

Recently, much attention has been devoted to a variety of networks that exhibit topological properties different from random graphs (for a review see Refs. [18–20]). For obtaining a detailed understanding of their architecture it has proved useful to trace the dynamics of the network's structural growth. As recently observed, major transitions in a systems dynamics can even be completely governed by preceding transformations in its network structure [15,16].

In the case of idiotypic networks (INW's) in the immune system [21], dynamics and network evolution are driven by a continuous influx of new idiotypes from the bone marrow. Data from experimental investigations suggest a daily bone marrow production only one order smaller than the actual network size [5,22,23]. A second principle governing the dynamics of INW's is a set of local rules: idiotypes die out if they are understimulated or overstimulated, i.e., have too few or too many neighbors. As Conway's famous "game of life" [24] suggests, systems governed by such local rules can evolve towards highly complex self-organized states [25].

Starting from a simple set of rules intending to mimic the dynamics within idiotypic networks in the immune system, we present a cellular automaton based model for the evolution of networks of occupied sites on graphs. Depending on the major parameter, the bone marrow influx, the model exhibits parameter regimes in which the system self-organizes into static and dynamic patterns, shows transitions between such ordered phases, and has a parameter range in which it is governed by randomness. We investigate these regimes and elucidate connections between the overall dynamics and the evolution of the network structure.

The organization of this paper is as follows. In the following section we introduce the model, give a brief introduction to idiotypic networks, and outline further possible applications of our model. Then, in Sec. III, we give an overview of the typical evolution of the initial dynamics of the population and its connection with changes in the network structure. Next, in Sec. IV the stationary state and its network organization will be characterized. In Sec. V the dependence of the system's qualitative behavior on the model's main parameter, the influx I, will be explored. In the same section, analytical results for small I derived from a microscopic view of the network characterizing fluctuations around the steady state will be presented and an explanation for the systems high I behavior will be given. In the final section changes in the variety of stationary network patterns for more closely linked base graphs will be discussed.

The aim of this paper is not finetuning or in detail matching of one of the applications, but rather generally exploring features of the dynamics caused by the window algorithm

and understanding its connection with network structures thus evolving.

II. THE MODEL AND SOME APPLICATIONS

Let G denote a lattice or, more generally, an undirected connected κ-regular graph (i.e., a graph, each of whose vertices is linked to κ neighbors). Let $v \in G$ denote the vertices or sites and the links between sites (i,j) within G be described by an adjacency matrix $\{m_{ij}\}_{1 \leqslant i,j \leqslant |G|}$. For simplicity, $m_{ij} \in \{0,1\}$ and $m_{ii}=0$. In the following G will also be called base graph. A vertex $v \in G$ can either be occupied or empty, i.e., have occupancy $s(v)=1$ or $s(v)=0$, respectively. Empty sites will be called holes. A vertex v with label i has an occupied neighbor degree $\partial v = \Sigma_{j=1}^{|G|} m_{ij} s(j) \leqslant \kappa$, counting the number of its occupied neighbors. We propose the following algorithm for an evolution of occupied and empty sites on G.

(i) Throw in I occupied vertices, i.e., select i holes randomly and let them become occupied. This supply of I new occupied vertices will be called influx.

(ii) Check the neighborhood of every site $v \in G$. If v is occupied and has occupied neighbor degree ∂v greater than t_u or less than t_l the vertex v will be set empty in the next time step. That is, $s_t(v)=1 \rightarrow s_{t+1}(v)=0$ if $\partial v < t_l$ or $\partial v > t_u$. The update of (i) and (ii) will be parallel.

(iii) Iterate (i) and (ii).
The threshold values t_l and t_u are model parameters, $t_l=0$ corresponds to no lower threshold at all. Thus, the main characteristic of the algorithm is a window of allowed occupied neighbor degrees. Hence we call it window algorithm. The graph of all occupied vertices after iteration t is finished will be denoted by $\Gamma_t \in G$ and $n_t = |\Gamma_t|$ will be called its population.

Note that in the first instance unlimited growth of the network is prevented by the upper threshold t_u. Once a stable structure has been established, there are no vertices violating the minimum occupied neighbor degree rule unless vertices are taken out because they got too many neighbors by the last influx. On the other hand, while t_u leads to an instantaneous removal of vertices due to the most recent influx, the lower threshold t_l can cause avalanches and is thus responsible for a memory of a perturbation which may last over several iterations. Such avalanches are thought to adjust the network structure.

These considerations make it also plain that for $t_u = t_l$ and $t_u = t_l + 1$ no long lasting populations can arise. In the first case, only a t_l regular graph Γ_t could be formed. Then already a small local reorganization would lead to an avalanche extinguishing the whole graph. In the second case, every vertex of Γ_t is critical in a sense that it is prone to being removed by a small perturbation caused by the influx.

Our main motivation to study such kind of dynamics for the evolution of networks comes from trying to model idiotypic networks INWs. The problem, however, appears to be far more general. Two other imaginable applications will also be sketched briefly: evolving networks of interacting species and, for conceiving a vivid picture of the above algorithm, a toy system of organzing coins in a box.

A. Idiotypic networks

Immune response against a broad class of antigens (bacteria, viruses, . . .) is triggered by antibodies and B cells (which carry only one type of antibody on their surface). Schematically this can be sketched as follows. Perchance the antigen encounters a shape- and charge-complementary antibody. Antibody and antigen thus form a complex that marks the antigen as hostile so that it will be removed by another functional group of cells (e.g., killer cells). If B cells, which carry exactly this type of antibody on their surface come into contact with such an antigen they become stimulated, multiply into a clone and finally become "production units" for this specific type of antibody.

It is the basic idea of idiotypic networks [21] that antibodies can not only recognize an antigen, but also complementary anti-antibodies (the specificities of both are then also called idiotypes). This leads to stimulation of the respective B cells and thus causes a kind of a permanent self-balanced immune activity independent of the hostile antigen.

These mutually recognizing idiotypes build the so-called idiotypic network. Its vertices or nodes are represented by idiotypes, its links by functional interactions between them. INW's are thought to play a role in, e.g., the preservation of idiotypic memory [21], the prevention of autoimmunity [26,27], the discriminization between self and nonself, and cancer control.

The interaction of idiotypes within the network can be described by Lotka-Volterra-like dynamics, i.e.,

$$\frac{dx_i}{dt} = x_i \left[-\gamma_i + f\left(\sum_j m_{ij} x_j \right) \right] + \xi_i, \qquad (1)$$

where i is an index labeling different idiotype populations, x_i the concentration of idiotype i, γ_i its inverse lifetime, f a so-called proliferation function describing the stimulation and death of B cells and antibody production by stimulated B cells, and ξ_i an influx rate of new idiotype species from the bone marrow. Since secreted antibodies and those on the surface of B cells are not explicitly distinguished, a description of INW dynamics as by Eq. (1) belongs to the category of A models [5]. Bone marrow production is thought to be uniformly distributed and random, i.e., there is a uniform probability for every idiotype that a member of its population is produced per unit of time.

It is a common approach to describe an idiotype or vertex v of the INW by a bitstring $(v_1, \ldots, v_d)$, $v_i \in \{0,1\}$ of length d [28]. Reasonable estimates for the number of possible idiotypes yield a bit-chain length of the order $d \approx 35$ [5]. Idiotypes interact if they are complementary. This is modelled by introducing "matching rules" that define when bit strings are connected in the above sense of complementarity. For instance, idiotypes can be said to interact if they are nearly exactly complementary or—in other words—the respective bit-strings match allowing for one deviating position, a mismatch, only. Generally, allowing bit strings with m

mismatches to interact, one obtains a $\kappa = \Sigma_{k=0}^{m} \binom{d}{k}$ regular graph $G_d^{(m)}$ whose links are described by an adjacency matrix with elements:

$$m_{ij}^{(m)} = \begin{cases} 1 & \text{if} \quad d_{\mathrm{H}}(i,\bar{j}) \leqslant m, \\ 0 & \text{otherwise,} \end{cases} \quad (2)$$

where $d_{\mathrm{H}}(i,j)$ is the Hamming distance between i and j, i.e., the number of digits, in which the bit chains differ. The better the matching of the corresponding idiotypes, the stronger the reaction affinities. In this respect, in the sequence $G_d^{(1)} \subset G_d^{(2)} \subset \cdots \subset G_d^{(m)}$ gradually smaller affinities are taken into account.

Sometimes it is also convenient to employ another view at the link structure of $G_d^{(m)}$. In the frame of these bit-string models every link is associated with a bit operation L, which, applied to one of the vertices that the link connects, yields the vertex at its opposite end. For links between vertices with ideally complementary bit chains i,j we have $j = L_0(i)$ (i is the inverse of j), for "one-mismatch links" $j = L_{k_1}(i)$ (i is obtained by inverting j and changing the bit at position k_1), for "two-mismatch links" $j = L_{k_1 k_2}(i)$, etc. Thus, in this sense, links are also labeled.

Using a discrete version of Eq. (1), idiotypes are either present ($x_i = 1$) or absent ($x_i = 0$). An idiotype v can survive if it, on the one hand, receives at least a minimum amount of stimulation from the network, but is not overstimulated on the other hand. Too high concentrations of antibody lead to each receptor of the B cell being bound to only one antibody. Since crosslinking of several antibodies is required in order to stimulate a B cell, [5] this leads to suppression of this idiotype's population. A more careful analysis yields that it is reasonable to assume that the proliferation function f is log-bell shaped. Then, from the steady state conditions of Eq. (1) one obtains a rough idea of the maximum and the minimum occupied neighbor degrees, t_1 and t_u. Normally, one matching antibody specificity is sufficient to cope with an antigen. Therefore in this model $t_1 = 1$, which defines the time scales for each iteration step.

B. Interacting species

A widely used approach to describe the interactions of species (macroscopic organisms, cells, reacting molecules, . . .) is by Lotka-Volterra-like dynamics of the type set forth in Eq. (1) [29]. The index i now distinguishes different species, x_i denotes their concentrations, $-\gamma_i > 0$ the net effect of death and birth rates, m_{ij} the adjacency matrix describing their interaction structure, and f a function modeling resource competition and the effect of predator-prey relations. Now, a species does not require a minimum amount of stimulation but is still going to be restrained by the effects of resource competition and prey. Thus, $t_1 = 0$ and $t_u > 0$. ξ in this context models a kind of mutation rate, which describes the appearance of new species. Unlike the case of bone marrow production, ξ is not uniform, but restricted to the neighborhood of already existing species and also much smaller.

Though probably hard to make out, G and m_{ij} describe the graph of all conceivable species and their potential interactions.

C. Coins in a box

Imagine a box and a heap of coins put inside initially. Then the box will be shaken, all overlapping coins be taken out, and randomly generated new heaps of coins be placed on randomly selected empty areas of the box. This procedure will be iterated several times. Clearly, in the above algorithm, the box corresponds to the base graph G, coins correspond to occupied vertices on G, and empty areas to holes. Overlapping coins have too many neighbors, thus too high an occupied neighbor degree and will consequently be taken out. Since also isolated coins are allowed to remain, the situation is that of $t_1 = 0$. t_u represents the maximum amount of coins that can be adjacent on a plane without overlap.

III. ANALYZING THE DYNAMICS

In this section we focus on analyzing the population dynamics and understanding corresponding changes in the network structure. Figure 1(a) shows a sample trajectory for the initial 300 time steps of the population dynamics for $(t_1, t_u) = (1,7)$ and $I = 10$ on a base graph $G_{12}^{(1)}$. As there seems to be a generic evolution with time it makes sense to look at averaged trajectories, i.e., $\langle n_t \rangle = \Sigma_n n p_t(n)$ where $p_t(n)$ denotes the probability that after t iterations n occupied vertices will be present [see Fig. 1(b)].

Clearly, several phases of the dynamics can be distinguished. First, it takes a certain time till accidentally at least a connected pair of occupied vertices is formed which then functions as a germ for further network growth.

To elucidate the structure of this germ for $t_1 > 1$ we define three subsets of a cluster C: (i) its (generalized) t_1-leaves $l_{t_1}(C)$, (ii) its (generalized) t_1-stem $s_{t_1}(C)$, and (iii) its (generalized) t_1-tree-reduced component $r_{t_1}(C)$. Leaves of the first generation are vertices of C with less than t_1 neighbors, i.e., $l_{t_1}^{(1)}(C) = \{v \in C | \partial v < t_1\}$. Then, leaves of the second generation $l_{t_1}^{(2)}(C)$ are vertices of $C \backslash l_{t_1}^{(1)}(C)$ with less than t_1 neighbors. (Here and in the sequel the symbol "$\backslash$" denotes the set theoretical difference.) Analogously, for $n = 2,3,\ldots,$ $l_{t_1}^{(n)} = \{v \in C \backslash l_{t_1}^{(n-1)} | \partial_{|C \backslash l_{t_1}^{(n-1)}} v < t_1\}$, where $\partial_{|C \backslash l_{t_1}^{(n-1)}} v$ denotes the number of occupied neighbors of v in $C \backslash l_{t_1}^{(n-1)}$. Thus, the treelike component of C is $t_{t_1}(C) = \cup_{j=1}^{\infty} l_{t_1}^{(j)}(C)$, the stem $s_{t_1} = t_{t_1} - l_{t_1}^{(1)}$, and the tree-reduced component $r_{t_1} = C \backslash t_{t_1}$. For $t_1 = 2$ these notions coincide with the usual definitions in graph theory.

Consider the application of the window algorithm with lower threshold t_1. If not sustained by random influx, the t_1 stem of a cluster is prone to successively fall victim to cascades in which the t_1 leaves are taken out first. Vertices that are critical, i.e., are still allowed, but will be removed if they lose a neighbor represent the $(t_1 + 1)$ leaves. On the contrary, the $(t_1 + 1)$-tree-reduced component is the subset not endan-
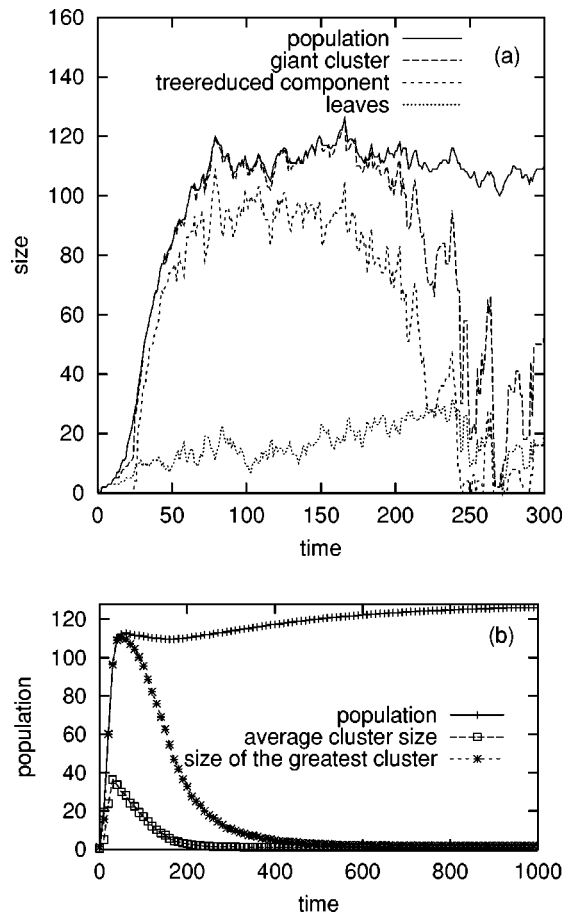
FIG. 1. (a) A sample trajectory for the population n_t, the giant cluster, the 2-tree-reduced component of the giant cluster ("backbone"), and its 2-leaves, see text. Parameters are $d=12$, $(t_1,t_u)=(1,7)$, and $I=10$. (b) Averaged trajectories of the population, the size of the greatest clusters, and the average cluster size versus time. Averages have been taken over 1000 independent runs; parameters are $d=8$, $(t_1,t_u)=(1,5)$, $I=6$.

gered by avalanches caused by critical vertices.

Apparently, the tree-reduced component of a cluster is invariant under step (ii) of the window algorithm. So, for $t_1 > 1$ in the above context the germ, which for $t_1=1$ is just a connected pair of occupied vertices, corresponds to a cluster with a nontrivial t_1-tree-reduced component. In case of, e.g., $t_1=2$ this is a 4-loop, for $t_1=3$ a cube, etc. The higher t_1 is, the more "organized" a germ is demanded and the longer it takes till it is formed perchance.

Initially, as this germ is still small it grows only slowly, since some of the new vertices are short of neighbors and thus are immediately taken out again. Then as a second phase of the dynamics a phase of almost linear growth of the population is entered. During this period almost all freshly thrown in vertices survive, since the network is already almost dense (thus providing enough neighbors), but still most of the vertices have only small occupied neighbor degree. As the number of vertices with higher occupied neighbor degrees increases, the growth of the population then abates and reaches a maximum. It can also be seen from Fig. 1(b) that during this phase almost all occupied vertices belong to one
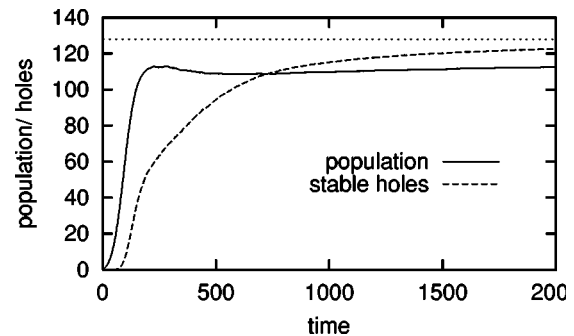

FIG. 2. Averaged trajectory (over 1000 independent runs) of the number of stable holes and of the population for $d=8$, $(t_1,t_u)=(1,5)$, $I=2$. The dotted line indicates half the system size $|G_8^{(1)}|/2=128$.

giant cluster. At the same time ($t\approx150$) as the maximum is reached, the giant cluster decays and small components start to split off. Interestingly, whereas in the initial stages of the dynamics the number of critical vertices is always of the same size as the influx, preceding the breakdown of the giant component more and more critical vertices are assembled [cf. Fig. 1(a)]. The maximum number of critical vertices is assumed at the same time ($t\approx240$) as the giant cluster breaks down.

The third phase now ensuing is marked by the complete decay of the giant cluster and a coinciding drop of the population. As soon as this is achieved the smaller fragments start becoming rearranged, again associated with an increase in the population.

Finally, the system saturates into a stationary state around which fluctuations occur. The higher t_u is, the more the population is allowed to grow initially and the more expressed the above described behavior becomes. Independent of the upper threshold, always half of the vertices are occupied in the final state. Recurring to clustering properties it turns out that average as well as maximum cluster sizes tend to 2.0. Thus, since there cannot be a cluster consisting of more than two occupied vertices this proves that for long times Γ_t completely decays into 2-clusters.

Holes play an important role in the systems' approaching the steady state. A hole h will be called stable if it has occupied neighbor degree $\partial h > t_u$. Clearly, unless it loses its property to be stable, a stable hole cannot become occupied. Reverting a stable hole back into a "normal" hole demands the removal of $\partial h - t_u$ of its occupied neighbors, which itself needs a rearrangement in the 1-neighborhood of these vertices.

From these considerations one realizes that—depending on the size of the neighborhood which has to be rearranged—there is a hierarchy of local structures with different (local) stability. "Normal" holes have least stability against random influx (they simply have to become occupied to change their state), then come occupied vertices (where a change of their occupancy needs a rearrangement of the 1-neighborhood), and most stable are stable holes (which need reorganizations of the 2-neighborhood).

Figure 2 shows an averaged trajectory for the evolution of the number of stable holes and the population size. Surpris-

ingly, even during the phase of declining population (which means that fewer occupied vertices to make a hole stable are available) the number of stable holes increases till finally in the steady state all holes tend to be stable. This can be understood from the above considerations. As described above in detail, the reversion of a stable hole into a normal hole requires occupied vertices in the neighborhood of the hole to be removed. However, the removal of vertices becomes more difficult the more stable holes are in their neighborhood. Thus, apparently, stable holes situated in each others (up to 2) adjacency can promote mutual stability. As a consequence of this a formation of almost "frozen" domains that are made of mutually stabilizing stable holes can be expected. These domains compete with each other and finally one of them prevails and fills the complete system. Indeed, the arrangement of occupied vertices and holes in the steady state exhibits patterns that will be discussed more closely in the following section.

IV. THE STATIONARY STATE

In order to characterize the network structure of the stationary state, every vertex $v \in G$ is assigned a mean-occupancy rate $\bar{s}(v) = 1/(T_1 - T_0)\Sigma_{t=T_0}^{T_1} s_t(v)$ and a mean switch rate $\bar{r}(v) = 1/(T_1 - T_0)\Sigma_{t=T_0}^{T_1}(1 - \delta_{s_t(v),s_{t+1}(v)})$. Mean-occupancy rate and mean switch rate give a measure of how many times a vertex is occupied or changes its occupation during the time interval $[T_0, T_1]$. T_0 will be chosen such that the system has already reached the stationary state. This method provides a way of obtaining an average picture of the occupation of G.

Figure 3 shows the mean occupancy rate and mean switch rate of every vertex after a simulation on $G_8^{(1)}$. Clearly, vertices with high-mean-occupancy rate have a low switch rate and vice versa. Thus, vertices that are frequently occupied tend to be occupied almost permanently; seldom occupied ones tend to be almost always holes.

To elucidate the structure of the network formed by the highly active vertices we define the subset $S(a) = \{v \in G | \bar{s}(v) > a\}$ containing all vertices that are more frequently occupied than with rate a.

In Fig. 4 the number of vertices belonging to $S(a)$ and the greatest connected cluster of $S(a)$ are shown as a function of the threshold value a. Due to the logarithmic scale a first drop from $|S(a)| = 256$ to $|S(a)| = 130$ at $a = 0$ is omitted. Two further thresholds become apparent: one at $a_1 \approx 3 \times 10^{-4}$ where the size of the greatest component of $S(a)$ rapidly drops to size 2 and a second one at $a_2 \approx 0.893$ which marks the decline in the distinction of high- and low-mean-occupancy vertices seen in Fig. 3.

In order to get rid of fluctuations occurring during the iterations, one can distinguish a set of high-mean-occupancy vertices $S_H = S(a_1)$ (which can be considered as permanently occupied) and a set $S_L = G \setminus S_H$ (corresponding to permanent holes) of vertices with low-mean occupancy. From Fig. 4 one derives further that S_L decays also into two groups, namely, a set S_{L_1} of 128 vertices with mean occupancy 0 and two
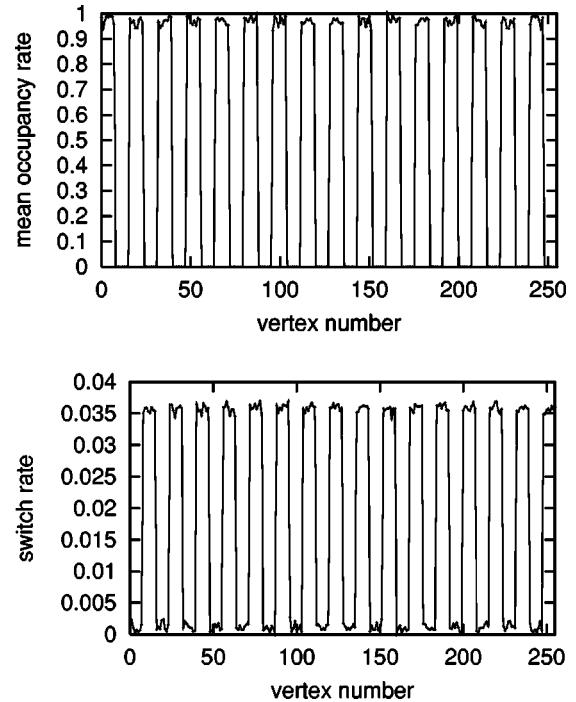

FIG. 3. Mean-occupancy rate and mean switch rate for every vertex after a simulation on $G_8^{(1)}$ with parameters $(t_1, t_u) = (1,4)$, $I = 5$. The relaxation time was chosen $T_0 = 10^4$, then averages over $T_1 = 9 \times 10^4$ time steps were taken. Bit strings $v = (v_1, \ldots, v_8)$ are uniquely represented by integers $z = \Sigma_{i=0}^{7} v_i 2^i$.

vertices (seen as a drop of $|S(a)|$ from 130 to 128 at $a = a_1$) with somewhat larger mean occupancy a slightly smaller than a_1. These two connected vertices having each $\kappa - 1 = 8$ neighbors from S_{L_1} are in the center of a starlike cluster of low-mean-occupancy vertices (cf. Fig. 5). They represent a vertex pair normally belonging to S_H which has accidentally been taken out and not got refilled yet. Thus they form a defect in the expression of a pattern structure (see Sec. V A).

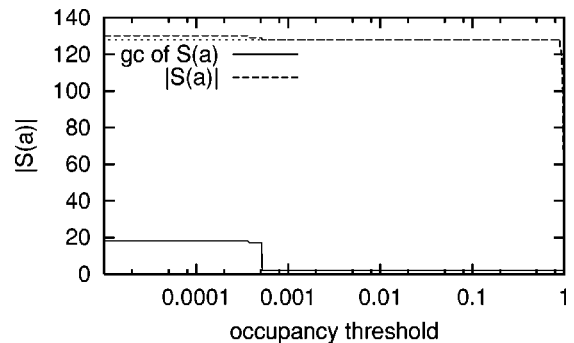

FIG. 4. Number of vertices belonging to $S(a)$ (see text) and the size of the greatest connected component of $S(a)$ as a function of the threshold a. Data are taken from simulations on $G_8^{(1)}$ with the window $(t_1, t_u) = (1,4)$ and influx $I = 5$. Due to the logarithmic scale the first point showing a drop of $|S(a)|$ from $|G| = 256$ to 130 is left out. The dotted line indicates the level $|S(a)| = 128$. Data have been assembled for $T_1 = 9 \times 10^4$ iterations after a relaxation time $T_0 = 10^4$.
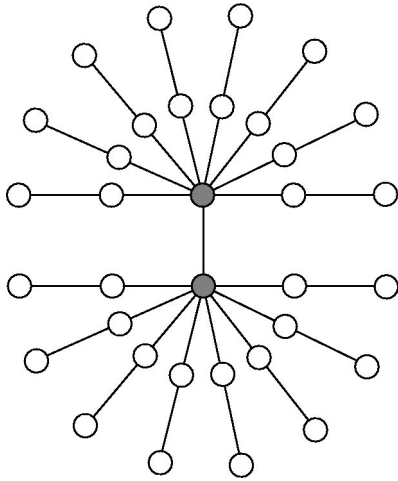
FIG. 5. Illustration of the cluster structure of the defect caused by the two vertices with mean occupancy rate $\bar{s} \approx a_1$ (drawn in gray) for $\kappa = 9$. These vertices are in the center of a starlike cluster of other low-mean-occupancy vertices from S_{L_1} (empty circles). For $a > a_1$ they no longer belong to $S(a)$ and thus their removal causes a decay of this cluster into ten 2-clusters of holes.

A further clustering analysis of S_H and S_L reveals that both subsets of G consist only of 2-clusters. Therefore, every vertex of $v \in S_L$ has exactly $\partial v = \kappa - 1$ neighbors from S_H and thus forms a stable hole of maximum possible stability. This justifies the above notion of a frozen domain.

In case of $t_u = \kappa - 1$ a holes being stable would require at least $\kappa = t_u + 1$ of its neighbors to be occupied. Due to the 2-cluster nature of the pattern, however, only $\kappa - 1$ neighbors are available, so that holes cannot be stable in this case. Patterns then become extremely transient in the sense discussed below in Sec. V B.

A. Metastable patterns and global stability

The actual steady state pattern, classified by groupings of vertices with clearly distinguished mean occupancy rates, depends on the influx I. If I is very small compared to the system size $|G|$, also patterns different from the 2-clustered pattern appear. The variety of such patterns is very abundant for $t_1 = 0$, becomes smaller the more restrictive the window is, and increases with decreasing ratio $I/|G|$.

They prove to be metastable, i.e., relax to a more stable pattern and finally to the 2-cluster pattern on very long time scales. Interestingly, for $t_1 = 0$ both sets S_H and S_L prove to have exactly alike properties and thus, the system is symmetric against an exchange of occupied vertices and holes [30].

Figure 6 gives examples for such a metastable pattern together with a visualization of the isomorphic graph structures of S_H and S_L. Typically, they consist of a large number of small clusters and few larger components. In the organization of the network structure of subclusters of S_H and S_L, basic units (e.g., 6-loops in Fig. 6) play a role. Nevertheless, the majority of the clusters turns out to be asymmetric.

In this context, a comparison to *random* graphs on G illustrates the very high organization of these patterns. A random graph $\Gamma \subset G$ (constructed by occupying vertices of G
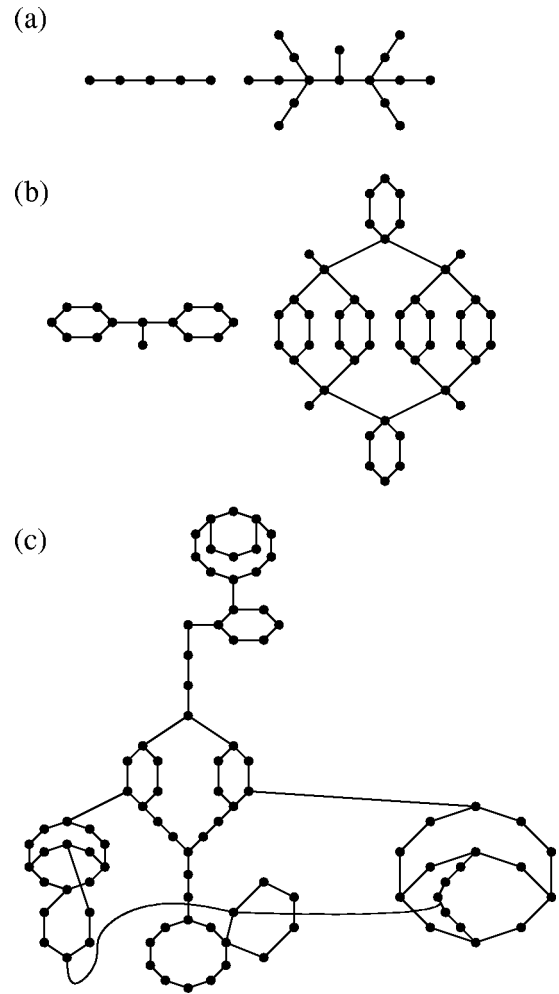

FIG. 6. Nontrivial clusters that appear in metastable patterns for $I = 5$, $(t_1, t_u) = (0, 7)$ on $G_{11}^{(1)}$. (a) 5- and 16-clusters from a pattern built by 192 singletons, 64 5-, and 32 16-clusters. (b) 14- and 44-clusters from a pattern with with 208 1-, 48 5-, 16 14-, and 8 44-clusters. (c) 2-tree-reduced component of the 203-cluster from a pattern consisting of 152 1-, 12 2-, 12 3-, and 4 203-clusters (2- and 3-clusters form chains). In the cases (a) and (b) larger clusters contain structures that resemble the smaller clusters. Larger loops, especially 6-loops and trees play a distinguished role. In all cases the dimension of the cluster structures is remarkably low.

with a uniform occupation probability p) will contain almost always only one giant connected component for $p > p_c \sim 1/\kappa$ [32]. Here, multiple giant components exist, although the fill ratio $|S_H|/|G| = 0.5$ far exceeds the percolation threshold.

Stability of a pattern is determined by the stability of its stable holes. Thus, a (rough) measure for the stability of a pattern is, e.g., the average occupied neighbor degree of its holes $\langle \partial v \rangle_{v \in S_L}$. It turns out that the holes in all these metastable patterns have an average occupied neighbor degree slightly smaller than that of the 2-clustered configurations.

Figure 7 shows another way to quantify stability. For this purpose we apply a test influx $\tilde{I}$. More specifically, a pattern P of holes and occupied vertices is taken, a number $\tilde{i} \leqslant |L|$ of its holes h belonging to the low-mean-occupancy set S_L ran-
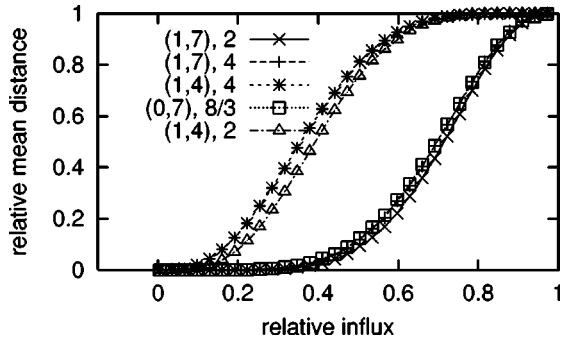
FIG. 7. Relative mean distance $\langle d(P,P')\rangle/|L|$ as a function of the relative influx $\tilde{I}/|L|$ for patterns that arise on $G_9^{(1)}$. Different lines correspond to patterns with different mean cluster sizes $\langle c\rangle$ which emerge for the given combinations of thresholds (t_1,t_u); see text. For the given relative influx, patterns are more stable the smaller their relative mean distance to the unperturbed pattern. Note that the data points marked by boxes and pluses almost coincide. Both patterns have the same mean occupied neighbor degree; see text.

domly selected and occupied, the window algorithm applied, and the distance $d(P,P')=\Sigma_{v\in G}|s_P(v)-s_{P'}(v)|$ between the original pattern and the resultant graph P' measured. Intuitively, $\tilde{I}$ is a measure for a perturbation that is applied to the pattern. A small mean deviation $\langle d(P,P')\rangle$ means a high stability against random influx $\tilde{I}$. For growing system sizes the sigmoid function $\langle d(P,P')\rangle/|L|$ tends to a step function.

Confirming the above ideas, Fig. 7 visualizes two tendencies: (i) an upper threshold $t_u<\kappa-1$ closer to $\kappa-1$ [33] and (ii) a higher mean occupied neighbor degree of holes $\langle\partial h\rangle_{h\in S_L}$ promote the stability of patterns. Indeed, patterns whose holes have the same mean occupied neighbor degree exhibit almost the same stability characteristics $\langle d(P,P')\rangle/|L|$. For example, holes in the patterns with $(t_1,t_u)=(0,7),\langle c\rangle=8/3$ and $(1,7),\langle c\rangle=4$ whose curves coincide in Fig. 7 (boxes and pluses) have both a mean occupied neighbor degree $\langle\partial h\rangle_{h\in S_H}=8.5$.

Due to the high supply of new idiotypes from the bone marrow these patterns are without interest for the purpose of modeling immune networks. However, it could be conceived that they prove interesting in the context of evolving species interaction networks where the influx as the mean number of new species per time unit is small in comparison to the overall network size.

B. Stable base configurations

The 2-clustered patterns are distinguished in two respects: (i) they are the only patterns evolving if the influx is high and (ii) they are stable, i.e., if once such a pattern is assumed the system will not relapse to one of the metastable patterns. Therefore we call these stable base configurations.

The complete decay of both hole and vertex configurations into 2-clusters allows it to calculate the multiplicity of these base configurations. It turns out that the global structure of a base configuration is already determined locally by fixing the occupancy s_0 of one connected pair of vertices. By

the knowledge of the 2-cluster structure of S_H and S_L one then knows that the vertices in the neighborhood of this pair have occupancy $s_1=1-s_0$. Thus, also the occupancy of their 2-cluster mates is fixed, which in turn determine the occupancy of vertices in their neighborhood and so on. By this argument every vertex's occupancy is uniquely determined since G is connected. All base configurations constructed in this way have been found to occur and are isomorphic to each other in the sense that without labeling vertices they cannot be distinguished.

As a consequence of the above argument, fixing s_0 and choosing one arbitrary vertex $o\in G$ and a link associated with a bit operation P leading to a two-cluster mate of o, $P(o)$, base configurations can be denoted by $B_{(s_0,P)}$. Hence, the number of possible base configurations is 2κ. The system is degenerate, though as $2\kappa/|G|\to0$ for $|G|\to\infty$ not macroscopically.

From a biological point of view it appears appealing to identify 2-clusters with idiotype–anti-idiotype pairs, the anti-idiotype playing the role of an internal image (memory) of a previously encountered antigen [21,34,35]. The 2-clusters found here, however, are "coherent" in a fixed pattern of a stable base configuration. This implies a maximum storage capacity 2κ which—also for large systems—is far too few to account for experimental observations.

It appears useful to consider distances between base configurations. One finds

$$d(B_{(s_0,P)},B_{(s_1,Q)})=\begin{cases} |G|/2 & \text{if } P\neq Q \text{ or } s_0\neq s_1, \\ |G| & \text{if } P=Q \text{ and } s_0=1-s_1, \\ 0 & \text{if } P=Q \text{ and } s_0=s_1. \end{cases}$$

(3)

Therefore, except the "inverse configuration," base configurations differ in exactly the half of their sites from all other base configurations. For the case $P\neq Q$ or $s_0\neq s_1$ half of the differing vertices are holes and half occupied vertices. Thus, the difference between base configurations is of the order of the system size and a change from one base configuration to another cannot take place without a major reorganization.

As the influx I increases occupied vertices become more and more prone to being removed. So, it can be expected that the distinction between frequently occupied and scarcely occupied vertices loses sharpness. Increasing I over a threshold leads to a completely different behavior of the system. Parameter regimes in which the system exhibits qualitatively different dynamics will be discussed in the following section.

V. DEPENDENCE ON THE INFLUX I

The systems behavior depends crucially on the clustering properties of Γ_t. To obtain a picture of the dynamics of cluster changes the time-averaged cluster size distribution over the interval $[T_1,T_0]$, $p(c)=1/(T_1-T_0)\Sigma_{t=T_0}^{T_1}p_t(c)$, where $p_t(c)$ denotes the probability that an arbitrary vertex of Γ_t belongs to a cluster of size c, has been investigated. Figure 8 shows numerical data for the cluster size distribution obtained for five different values of I. For small influx
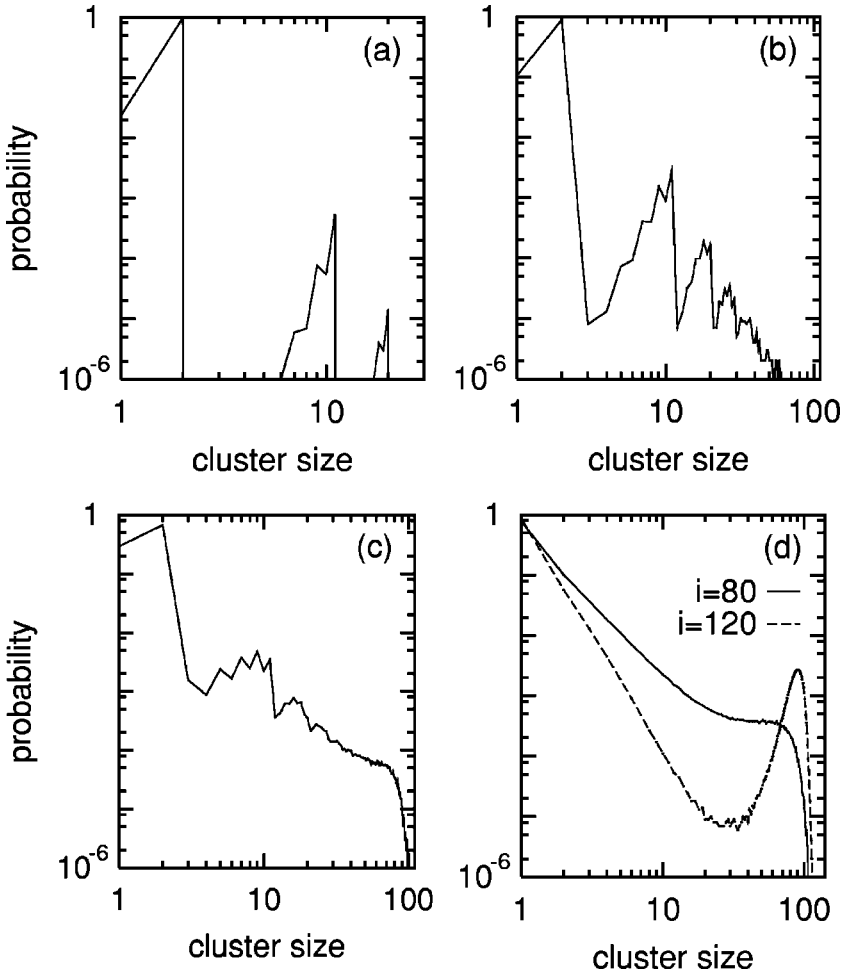
FIG. 8. Numerical data for the cluster size distribution $p(c)$ for different influxes $I=20$ (a), 30 (b), 40 (c), 80, and 120 (d) corresponding to different regimes as described in the text. Simulations were performed on $G_8^{(1)}$ with $(t_1, t_u) = (1,5)$.

$I=20$ [Fig. 8(a)] the systems' behavior is dominated by the occurrence of 2-clusters. Occasionally also other clusters of sizes $c=6,\ldots,11$ and sizes $c=16,\ldots,20$ appear. For $I=30$ [Fig. 8(b)] the distribution has a structured tail of series of local extrema. Then, for $I=40$ [Fig. 8(c)] the 2-cluster dominated structure is still expressed, but now also clusters some orders of magnitude larger are found. Finally, for $I=80$ and $I=120$ [Fig. 8(d)], the clustering structure is dominated by (depending on t_1 and t_u) one or several giant clusters and 1-clusters (singletons) which more and more outweigh other small clusters as I is further increased. $I=20$, 40, and 80 represent three different parameter regimes for the influx that will be treated below.

A. Small I: A statistical approach of defects

For small I during the initial stages of the dynamics the 2-cluster dominated pattern as described in Sec. IV B is formed. Once such a pattern is established I works as a perturbation that incidentally causes defects to the ideal pattern structure. These defects can be classified into two groups: "hole" defects and "vertex" defects (cf. Fig. 9). Both terms arise from a comparison between the perturbed configuration Γ_t at time t and the base configuration B the system is in. By the term vertex defect we understand a vertex that is occupied in B, but empty in Γ_t. Likewise, a hole defect is a vertex that is empty in B, but occupied in Γ_t. Clearly, hole defects are caused by $\kappa - 1 - t_u$ correlated vertex defects and thus are much less probable than vertex defects. As long as only vertex defects occur only 1- and 2-clusters can be formed. However, once a hole defect is established, it serves as a junction for its surrounding 2-clusters and clusters of size $2\nu+1$, $\nu=1,2,\ldots,\kappa$ are built. For example, in Fig. 8(a), local maxima are found for $c=7,9$, and 11. The latter one corresponds to the most probable kind of hole defect: a formerly stable hole now is occupied and has five remaining occupied neighbors. In the case of the less probable cluster of size $c=9$ four once occupied neighbors of the hole are defective, thus four are remaining. Analogously for $c=7$. As the 2-clusters surrounding a hole defect might also be defective though less frequently also clusters of even size appear. The second series of local maxima around $c=20$ in Fig. 8(a) can be explained by hole defects that are correlated, i.e., hole defects whose occupied 2-cluster neighbors are connected.

This microscopic picture of the process suggests a treatment borrowed from equilibrium statistical mechanics. Since defects are more likely to occur for higher influx, I can be associated with a kind of a "temperature" $T(I)$. $T(I)$ will be growing monotonically with I. Defects are assigned an "energy" $\alpha(t_u)$ that describes the probability that a defect is caused. Since it is harder to remove occupied vertices the higher t_u is, it is also expected that α grows with increasing upper thresholds t_u.
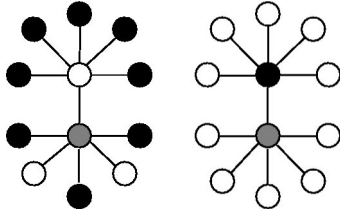
FIG. 9. Illustration of "hole defects" (left) and "vertex defects" (right) for $(t_1, t_u) = (0,4)$. The defective vertex is printed in gray, holes in white, and occupied vertices in black. On the left hand side, one of the central holes has $5 > t_u$ occupied neighbors and thus is stable. The gray hole has lost two of its neighbors due to "vertex defects." Only $3 < t_u$ neighbors remain so that the gray hole has lost its stability and can be occupied. Both unstable and occupied holes are called hole defects. On the right hand side, the gray vertex was removed, thus causing a defect to the ideal 2-cluster pattern structure.

In the following we derive a statistical description for an ideal gas of defects.

1. The case $t_1 = 0$

The probability to cause a vertex defect depends on the number of holes surrounding the occupied vertex. In spite of this no distinction between defects of completely removed 2-clusters and singletons will be made. This is justified since for large systems an occupied vertex that remains after its 2-cluster mate has been removed is still surrounded by almost the same number of holes. Furthermore, for $t_1 = 0$ the algorithm allows the permanent existence of singletons.

The probability of having l independent defects of energy α at temperature $1/\beta(I)$ in an ideal pattern of $N = |G|/2$ occupied vertices is

$$p(l) = \frac{1}{Z} \binom{N}{l} e^{-l\beta\alpha}, \qquad (4)$$

where the partition sum Z is easily determined as

$$Z = \sum_{l=0}^{N} \binom{N}{l} e^{-l\beta\alpha} = (1 + e^{-\beta\alpha})^N. \qquad (5)$$

Then the mean number of defects is given by

$$\langle l \rangle = -\frac{1}{\beta} \frac{\partial \ln Z}{\partial \alpha} = N - \langle n \rangle = N \frac{e^{-\beta\alpha}}{1 + e^{-\beta\alpha}}, \qquad (6)$$

$\langle n \rangle$ being the mean number of actually occupied vertices.

Comparing with data obtained from simulations it turns out that the ansatz $1/\beta = I_0 + I$ holds for a broad range of different values of I. From a fit of the mean populations with Eq. (6) one obtains $\alpha = 88.14 \pm 0.48$ and $I_0 = 0.67 \pm 0.18$. In the whole range up to $I < 35$ mean values and probability distributions calculated by Eq. (4) are in good agreement with simulations (see Figs. 10 and 11).

For very small I it is by simple combinatorics possible to obtain an approximation for the "energies" fitted from the data of Fig. 10. If for fixed t_u the influx I is so small that it
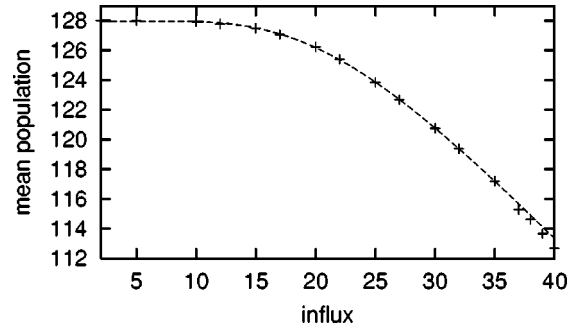

FIG. 10. Mean population $\langle n \rangle$ versus influx I taken from simulations for $(t_1, t_u) = (0,5)$ on $G_8^{(1)}$. The crosses represent simulation data; the line corresponds to a fit of $\langle n \rangle$ calculated from Eq. (6). Fit parameters are $\alpha = 88.14$ and $I_0 = 0.67$.

can cause not more than exactly one vertex defect, i.e., $I < 2(t_u + 1)$, the probability per site for a defect is [31]

$$p_d(I) = \binom{N}{I}^{-1} \sum_{j=t_u}^{\kappa-1} \binom{I}{j} \binom{\kappa-1}{j} \binom{N-(\kappa-1)}{I-j}. \qquad (7)$$

If no more than one defect can arise, the mean number of defects is given by $\langle l \rangle(I) = N p_d(I)$. Using Eq. (7) one calculates $p_d(t_u)$ and $p_d(t_u + 1)$. A comparison with Eq. (6) yields

$$\alpha^{-1} \approx [\ln p_d(t_u)]^{-1} - [\ln p_d(t_u + 1)]^{-1}, \qquad (8)$$
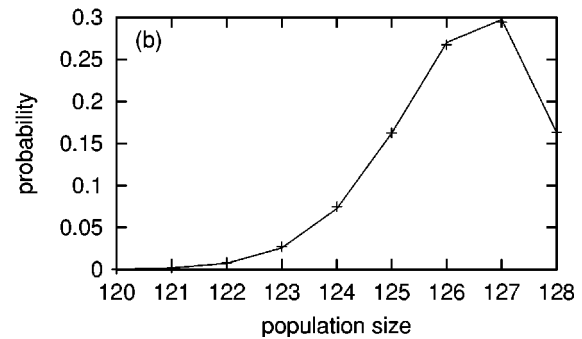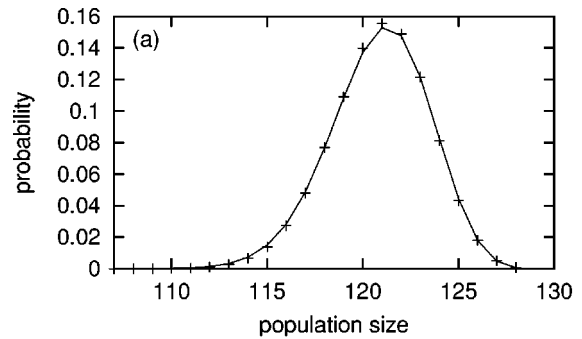

FIG. 11. Probability distributions $p(n) = 1/(T_1 - T_0) \Sigma_{t=T_0}^{T_1} \Sigma_n n p_t(n)$ for the population size obtained from simulations on $G_8^{(1)}$ for $(t_1, t_u) = (0,5)$ and $I = 30$ (a) and $I = 20$ (b). The simulation results (crosses) are compared with $p(N-n)$ from Eq. (4) (lines connect calculated points) using $\alpha = 88.14$ and $I_0 = 0.67$.

which, e.g., evaluated for $d=8$ and $t_u=5$ gives $\alpha=50.8$, which is of the same order as the numerical value $\alpha=88.14$. Comparing I_0 is not reasonable, since Eq. (6) bears deficits for small influxes.

Indeed, the range of validity of Eq. (6) is limited in two respects. First, although the possible number of defects for small I is limited by $\lfloor I/t_u \rfloor$ the sum in Eq. (5) extends up to N. However, for low temperatures surplus defects are counted with only a small statistical weight. This approximation becomes worse for high upper thresholds t_u. Second, too many vertex defects (which then become correlated) lead to hole defects. Hole defects destabilize the 2-cluster pattern and lead to a qualitative change of the above picture.

2. The case $t_1=1$

For $t_1=1$ a distinction between two types of vertex defects becomes necessary. Now, unless a new 2-cluster mate is provided by fresh influx during the next iteration, a singleton violates the lower threshold rule. Hence it can only survive for one time step.

To cope with this situation in the present framework defects consisting of a singleton (α defects) are assigned an energy α, defects made of a completely removed 2-cluster pair (γ defects) an energy γ. Both energies are expected to increase with growing bit-chain length d and for higher upper thresholds t_u. Then a configurations energy with l_1 α and l_2 γ defects is $E(l_1,l_2)=l_1\alpha+l_2\gamma$.

The probability of having l_1 independent α and l_2 γ defects is

$$p(l_1,l_2)=\frac{1}{Z}\binom{N/2}{l_1}\binom{N/2-l_1}{l_2}2^{l_1}e^{-l_1\beta\alpha}e^{-l_2\beta\gamma}. \quad (9)$$

For the partition sum one obtains

$$Z=\sum_{l_1=0}^{N/2}\binom{N/2}{l_1}2^{l_1}e^{-l_1\beta\alpha}\sum_{l_2=0}^{N/2-l_1}\binom{N/2-l_1}{l_2}e^{-l_2\beta\gamma}$$

$$=(1+2e^{-\beta\alpha}+e^{-\beta\gamma})^{N/2}. \quad (10)$$

In analogy with Eq. (6) one derives the mean number of α defects,

$$\langle l_1\rangle=N\frac{e^{-\beta\alpha}}{1+2e^{-\beta\alpha}+e^{-\beta\gamma}}, \quad (11)$$

and obtains the mean number of γ defects,

$$\langle l_2\rangle=\frac{N}{2}\frac{e^{-\beta\gamma}}{1+e^{-\beta\gamma}+2e^{-\beta\alpha}}. \quad (12)$$

Finally, the number of empty vertices is $n=N-l_1-2l_2$, and hence the mean population is given by

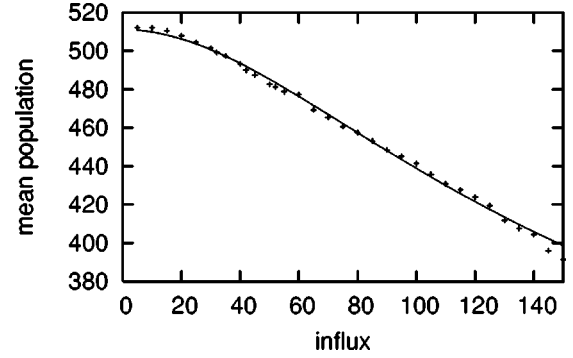$$\langle n\rangle=N\frac{1+e^{-\beta\alpha}}{1+e^{-\beta\gamma}+2e^{-\beta\alpha}}. \quad (13)$$

FIG. 12. The mean population for $G_{10}^{(1)}$ with $(t_1,t_u)=(1,5)$. Fitting with Eq. (13) leads to $\alpha=632\pm99$, $\gamma=250.6\pm13.1$, and $I_0=36.1\pm4.2$. The fit breaks down if one tries to include the range $I\geq150$ that marks the onset of the transition region (see Sec. V B).

The ansatz $1/\beta=I_0+I$ is again confirmed by a comparison of Eq. (13) with numerical data for the mean population (see Fig. 12). The probability distribution that n vertices are occupied at a time t is

$$\text{prob}\{n \text{ occupied vertices}\}=\sum_{l_2=0}^{l_{max}}p(N-n-2l_2,l_2), \quad (14)$$

where $l_{max}=\lfloor N/2-n/2\rfloor$ and $p(l_1,l_2)$ as given by Eq. (9).

Analytical results derived from Eq. (14) are again in good agreement with simulation data (see Fig. 13). Equations (13)
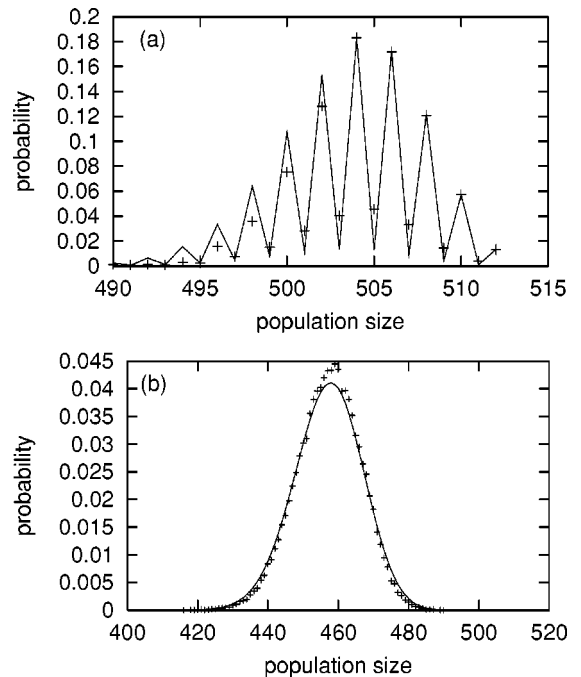

FIG. 13. Comparison between simulation data for the probability distributions of the population size for $G_{10}^{(1)}$, $(t_1,t_u)=(1,5)$ (a) $I=25$ and (b) $I=80$ and results derived from Eq. (14) for the same α, γ, and I_0 as in Fig. 12. In (b) the influx is already high enough that both types of defects appear with almost equal probabilities.
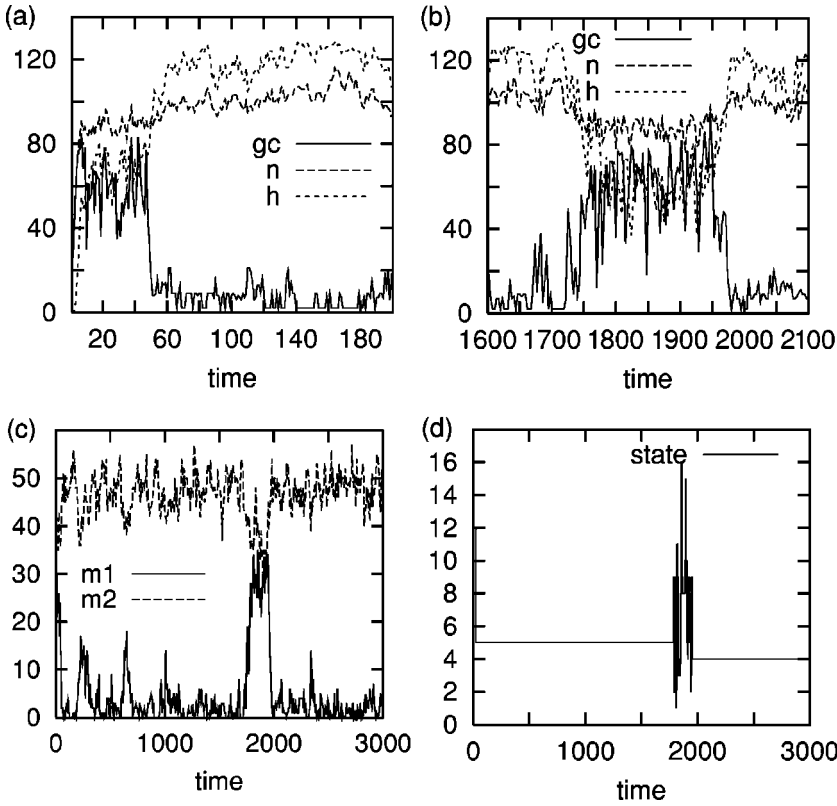
FIG. 14. Simulation data for $G_8^{(1)}$, (t_1,t_u) $=(1,4)$. (a) shows the population n, the number h of stable holes, and the size of the greatest connected component of Γ_t, gc. Initially, approximately half of all sites on $G_8^{(1)}$ become stable holes and a pattern is assumed. (b) shows a transition period. The number of stable holes h and the population n drop suddenly, a giant cluster is formed. (c) shows the smallest and the second smallest distance to a stable base configuration m_1 and m_2 (cf. text). In the transition period no pattern is selected. (d) displays a number for the pattern that has the smallest distance to Γ_t. In the transition period between two sharply assumed patterns the state changes quickly. For $t \in [200,1700]$, $k_{min}=5$, for $t>2000$, $k_{min}=4$.

and (14) are subject to the same limitations as in the case for $t_1=0$.

B. The transition region

As previously discussed increasing I beyond a threshold leads to a growing number of hole defects. The appearance of correlated hole defects is connected with the formation of great clusters consisting of connected 2-clusters. As I becomes still larger, the probability that hole defects become correlated increases. Occasionally this leads to the emergence of a giant cluster (see Fig. 8, the different series of local maxima correspond to an increasing number of connected hole defects). Speaking in the language of thermodynamics, growing influx entails a growth of fluctuations that finally tend to overthrow the regular pattern structure.

The building of a giant cluster requires the reversion of a major fraction of the stable holes into normal holes. Thus, since stable holes form the "skeleton framing" of the pattern structure, the system relapses into a phase where no pattern lasts for a longer time span.

Figure 14 illustrates this behavior for a simulation on $G_8^{(1)}$ with $(t_1,t_u)=(1,4)$. Initially, after the first stages of the dynamics the system settles into a steady state. For better illustration every stable base configuration $B_{(s_0,P)}$ is given a unique number k, $k=1,\ldots,18$. In Fig. 14(c) the minimum distance

$$m_1=\min_k d(\Gamma_t,B_k) \qquad (15)$$

and the second smallest distance

$$m_2=\min_{k \neq k_{min}} d(\Gamma_t,B_k) \qquad (16)$$

to any stable base configuration are shown. For the time intervals $[200,1700]$ and $[2000,3000]$ it holds $m_1 \ll m_2$. Consequently the system is in the stable base configuration $B_{k_{min}}$. Incidentally, hole defects associated with the emergence of larger clusters appear. Mostly, as long as hole defects remain uncorrelated, they are repaired during the next iterations. At $t \approx 1700$ the exact lock in of state $k_{min}=5$ is lost and for $t \in I_{change}=[1700,2000]$ a phase marked by frequent changes of k_{min} is entered. During this period $m_1 \approx m_2$ and thus no base configuration is sharply assumed. A comparison of vertex mean occupancy rates during this phase and the previous one justifies to speak of the time interval $t \in I_{change}$ as of a disordered period, since, clearly, any distinction between high-mean-occupancy and low-mean occupancy vertices is lost (see also Fig. 15). As expected, the emergence of the disordered phase goes hand in hand with the formation of a giant connected component in Γ_t, a drastic loss of stable holes, and a drop in the population.

The whole dynamics of the system is marked by a sequence of ordered and disordered phases. As I is increased, the residence time in ordered phases declines till finally the frequency of "base configuration" changes (defined as a change of k_{min}) tends to 1. Thus, the system becomes completely disordered.

Figure 16 displays simulation data on $G_{10}^{(1)}$ with (t_1,t_u) $=(1,8)$ for the mean time (residence time) during which k_{min} remains unchanged. An abrupt transition from a phase marked by permanent patterns to a phase of transient patterns
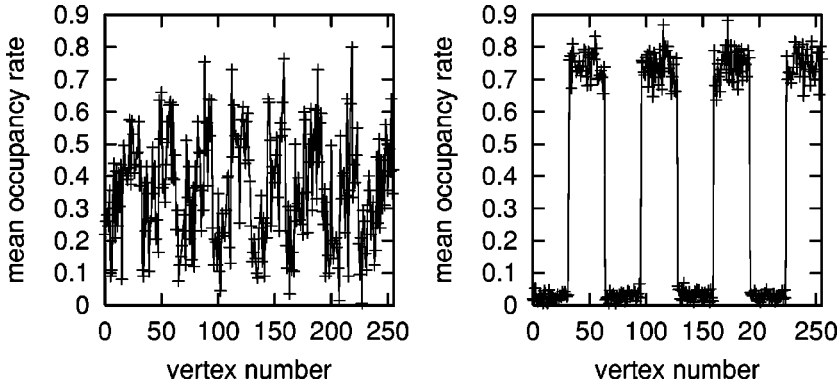
FIG. 15. Comparison between the mean occupancy distributions measured in a transition period (left) and during the time before the transition period (right). In the right hand figure a 2-clustered pattern is assumed. Same parameters as in Fig. 14.

interrupted by periods of disorder occurs at $I_c \approx 270$. Accordingly, as can be seen from Fig. 17, the mean lifetime (averaged over all vertices) drops abruptly during this range of influxes. For $I > 300$ mean lifetimes decay exponentially and quickly tend to 1. Very short lifetimes, however, do not allow for static order or memory. Apparently, the transition from order to disorder goes through a phase of more and more frequent pattern changes.

C. High $I > I_c$: Iterated maps

For influxes $I > I_c$ the lifetime of occupied vertices becomes very short. This indicates that the system can no longer form ordered patterns and long-time correlations between the systems configurations disappear. Thus, while for low influx clearly $\langle n_{t+1} \rangle$ is an intricate function of both the systems configuration Γ_t at time step t and the most recent influx, for high influxes the mean population at time step $t+1$ tends to depend only on the size of I and the mean population at the previous time step. Also, from the mean occupancy distributions one conjectures that the structure of Γ_t is essentially random, i.e., obtained by randomly occupying $|\Gamma_t|$ vertices of the base graph G.

If one randomly occupies n sites of a base graph G the relative mean number $h(n)$ of occupied sites after sites with occupied neighbor degrees outside of (t_1, t_u) have been removed is given by

$$
h\left(\frac{n}{|G|}\right) = \begin{cases} \dfrac{n}{|G|} \displaystyle\sum_{l=t_1}^{t_u} \binom{\kappa}{l} \left(\dfrac{n}{|G|}\right)^l \left(1 - \dfrac{n}{|G|}\right)^{\kappa - l} & \text{if } n < |G| \\ 0 & \text{otherwise.} \end{cases}
$$
(17)

Considering a large random influx, apart from fluctuations the relative population x_t will evolve according to $x_{t+1} = h(I/|G| + x_t)$. Thus, in the steady state x will preferably assume values near the stable fixed points of the shifted function $g(x) = h(I/|G| + x)$, i.e., near the solutions of $x^* = g(x^*)$. Linear stability analysis yields that a fixed point is stable if $|g'(x^*)| < 1$. Analogously, n cycles $\{x^*, g(x^*), g^{(2)}(x^*) = g(g(x^*)), \dots, g^{(n-1)}(x^*)\}$ are solutions of $g^{(n)}(x) = x$ and are stable if $|g^{(n)\prime}(x^*)| < 1$.

For $\kappa = 11$ and $(t_1, t_u) = (1, 8)$ $g(x)$ is a function with one maximum. Consequently, one expects that $g^{(n)}$ has at most n maxima. Thus, in principle, cycles of higher order are possible.

The function $g(x)$ is a polynomial of order t_u. Thus $g^{(n)}$ is of order t_u^n and there is no general analytic solution to $x^* = g^{(n)}(x^*)$. As an example we consider the case $(t_1, t_u) = (1, 8)$ on $G_{10}^{(1)}$, i.e., $\kappa = 11$ and $|G| = 1024$. Evaluating the fixed point equations numerically, one obtains the bifurcation diagram displayed in Fig. 18. At $x = 0.2$ one finds a forward pitchfork bifurcation towards a 2-cycle, which then at $x = 0.3$ becomes also unstable, leading to the emergence of a 4-cycle. For $x = 0.45$ this 4-cycle is found to become unstable and a backward pitchfork bifurcation leads again to a stable 2-cycle. Far outside the region of biological interest, for $x = 0.93$ a backward bifurcation occurs and the single fixed point solution again becomes stable. Figure 18 also displays data obtained from simulations of the window algorithm on $G_{10}^{(1)}$ which exhibit the same qualitative behavior as the iteration of g. As expected, deviations become small as I increases.

VI. MORE DENSELY WIRED SYSTEMS: TWO-MISMATCH BASE GRAPHS

In this section some observations about the dynamics created by the window algorithm with $t_1 = 1$ on more densely wired base graphs will be presented. As a consequence of a higher coordination number different static patterns and several dynamic patterns can be observed. In principle, we expect (i) more sparsely populated, and hence transient patterns of reduced stability for low t_u and (ii) enhanced stability for upper thresholds close to $\kappa - 1$ (cf. Sec. IV A).

As an extension of the base graphs $G_d^{(1)}$ whose link structure is created by "one-mismatch links" we now introduce additional links connecting bit chains that deviate in two positions from complementarity, so defining the base graphs $G_d^{(2)}$, cf. Eq. (2).

Clearly, since $G_d^{(1)}$ is connected such "two-mismatch links" of $G_d^{(2)}$ are shortcuts of paths in $G_d^{(1)}$. For example, referring to the notion of bit operations associated with links (see Sec. II A), two vertices linked by $L_{k_1 k_2} \in G_d^{(2)}$, $k_1 \neq k_2$, are also linked by the six paths corresponding to combinations of the edges L_0, L_{k_1}, $L_{k_2} \in G_d^{(1)}$.

Although every vertex now acquires $d(d-1)/2$ new edges the former link structure is conserved. Thus, it could be conceived that patterns created on $G_d^{(2)}$ retain a part of the structure of the stable base configurations that are formed on
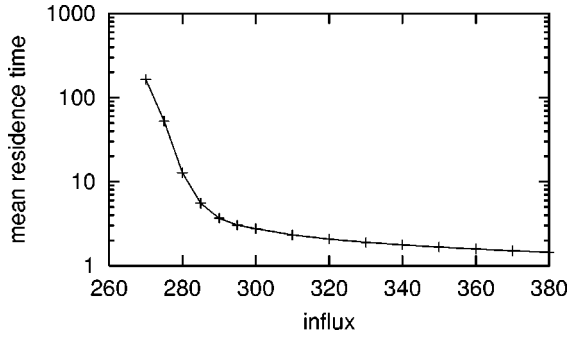
FIG. 16. Mean residence time, i.e., time during which k_{min} remains unchanged (excluding a relaxation time of the first 5000 time steps). All simulations on $G_{10}^{(1)}$ with $(t_1, t_u) = (1,8)$ have been allowed to run for 10^5 time steps. For $I < I_c = 270$ no change of k_{min} has been found.

$G_d^{(1)}$. Counting, e.g., "two-mismatch" links in a base configuration $B_{(s_0, F_1)} \subset G_d^{(1)}$ one finds that every occupied vertex now acquires d new links on $G_d^{(2)}$ (cf. Fig. 19), aggregating to a total occupied neighbor degree $d + 1$. Thus, these kind of patterns are forbidden for $t_u < d + 1$. For $t_u \geq d + 1$, however, it turns out that apart from metastable structures for small influx the dynamics always ends up in the above described configurations. Thus, in this case the base graph $G_d^{(2)}$ always decays into two groups of high-mean-occupancy vertices S_H and low-mean-occupancy vertices S_L. Both S_H and S_L form $(d+1)$-regular subclusters of $G_d^{(2)}$. Resuming the considerations of Sec. IV B one finds that these stable base configurations on $G_d^{(2)}$ have multiplicity $2d$. The scenario for growing influx is the same as on $G_d^{(1)}$: for $I > I_c$ phases of well-defined base configuration are interrupted by disordered periods leading to pattern changes, and finally to a dynamics marked by randomness and very short lifetimes.

However, for $t_u < d + 1$ where "relics" of patterns forming on $G_d^{(1)}$ are no longer allowed the behavior turns out to be more interesting.

As tools to investigate the structure of networks we again consider the mean occupancy rates of all vertices and probe
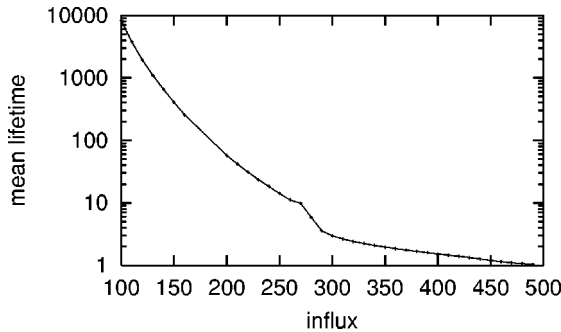

FIG. 17. Mean lifetime versus influx I obtained from simulations on $G_{10}^{(1)}$ for $(t_1, t_u) = (1,8)$. The mean lifetime was determined after allowing 5000 time steps for relaxation to a steady state. For every I the simulations then run for 95 000 more iterations. Data for $I < 100$ are not shown since mean lifetimes exceeded simulation times.
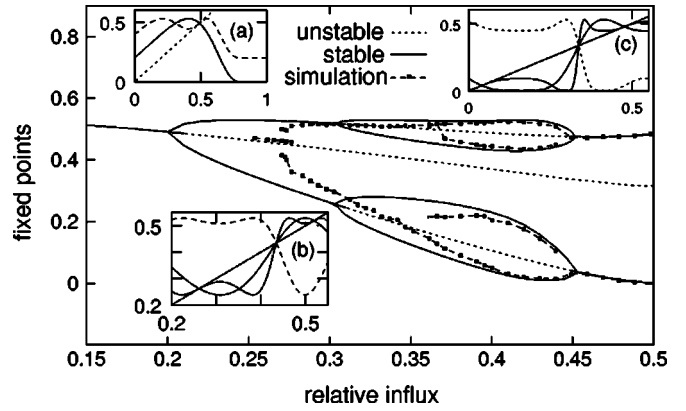

FIG. 18. The bifurcation diagram obtained by iterating the function $g(x)$ in comparison to simulation results for the maxima of the population histogram for $(t_1, t_u) = (1,8)$ on $G_{10}^{(1)}$ (filled squares connected by lines). Solid lines correspond to stable branches and dashed lines to unstable branches. The region of the simulation data where three stable solutions coexist corresponds to the onset of disorder: The intermediate branch represents the mean population during periods in which the system closely assumes a base configuration; the upper and lower branches are data sampled during disordered phases. Especially for higher influx, simulation results and the data obtained by iterating g are in very good agreement. The smaller diagrams visualize changes in the stability of fixed points of g at the branching points: (a) g (solid line) becomes unstable at $I/|G| = 0.2$, but $g^{(2)}$ (dashed line) is stable. Hence a cycle appears. (b) At $I/|G| = 0.3$ also $g^{(2)}$ (solid line) becomes unstable and—since $g^{(3)}$ (dashed line) gives only one unstable solution—a 4-cycle emerges. (c) At $I/|G| = 0.45$ $g^{(2)}$ becomes stable again leading to a backward bifurcation and a 2-cycle.

the mean-occupancy-patterns by defining subsets $S(a) \subset G_d^{(2)}$ with different threshold-occupancy rates a (see Sec. IV). In analogy with results for the one-mismatch case we find metastable patterns for small influxes. Depending on the ratio $I/|G_d^{(2)}|$, first completely 2-clustered, 4-clustered, or 8-clustered patterns appear (4-clusters are chains, 8-clusters cubes). Next in a range of influxes cube-configurations dominate (cf. Fig. 20). Different from the 2- and 4-cluster patterns, however, the cubes do not fill the base graph completely and 256 vertices not matching in the cube pattern are left.

Figure 21 shows data for every vertex's mean occupancy obtained by a simulation on $G_{12}^{(2)}$ with $(t_1, t_u) = (1,10)$. The set of vertices with highest mean occupancy S_H decays into cubes, the set with lowest mean occupancy S_L forms a giant component of 2816 vertices. S_L consists of 1536 almost never occupied vertices of occupied neighbor degree $\partial_{|G \setminus S_L} = 61$, 256 with $\partial_{|G \setminus S_L} = 43$ and 1024 with $\partial_{|G \setminus S_L} = 39$. All occupied neighbor degrees are larger than t_u and thus S_L entirely consists of stable holes. The 256 vertices not exactly matching in the cube pattern form a subset S_M of intermediate mean occupancy. S_M turns out to contain only singletons, each of which is surrounded by elements of S_L which are almost never occupied. Thus, vertices of S_M are isolated spots of activity sustained by influx temporarily placed at their surrounding stable holes, but taken out immediately af-
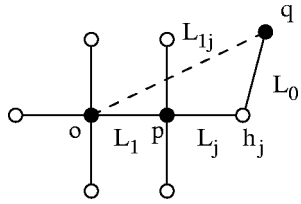
FIG. 19. An illustration of how "two-mismatch links" (dashed line) contribute to the occupied neighbor degree of occupied vertices in a base configuration $B_{(s_0,L_1)}$. Occupied vertices in $B_{(s_0,L_1)}$ are drawn in black, empty ones in white. Two clusters (e.g., o and p) in B are connected via the "one-mismatch link" (solid line) L_1. Except o the one-mismatch neighbors $h_j = L_j(p)$, $j \neq 1$, of p are holes. Apart from the holes' 2-cluster mates $L_1(h_j)$ all their neighbors are occupied. If one pursues an inversion link L_0 from any such hole h_j adjacent to p, a vertex $q = F_0(h_j)$ is reached which is—via L_{1j}— also a two-mismatch neighbor of o. One can easily verify that o has no other occupied "two-mismatch neighbors." Consequently, in a base configuration B on $G_d^{(2)}$ every occupied vertex has $d+1$ occupied neighbors.

terwards due to overstimulation. Consequently, as long as no fresh influx is placed adjacent to it in the next time step a vertex of S_M dies out one time step after it has been inserted. This view is confirmed by very short mean lifetimes $\langle T_{\text{life}} \rangle_{S_M} \approx 1$ of elements of S_M, which slightly grow with increasing influx. Together with a growing probability that isolated holes get filled this accounts for relatively large mean occupancies $\langle s \rangle_{S_M}$ in comparison to $\langle s \rangle_{S_L}$. Though at the first glance it seems surprising that a vertex can survive at a site where it is surrounded by almost always empty sites, this indicates a mechanism that is to prevail in a consecutive regime: isolated vertices of high durability are sustained by quickly fluctuating short-living influx in their neighborhoods.

Increasing I over approximately 80 the cube patterns become unstable and from $I \approx 100$ onwards a pattern marked by six-levels of mean occupancy (see Fig. 22) is chosen. In contrast to the appearance of several levels of mean occupancy due to transitions between isomorphic stable base configurations this grouping is of a different nature. While in the first case simulations started with different initial conditions
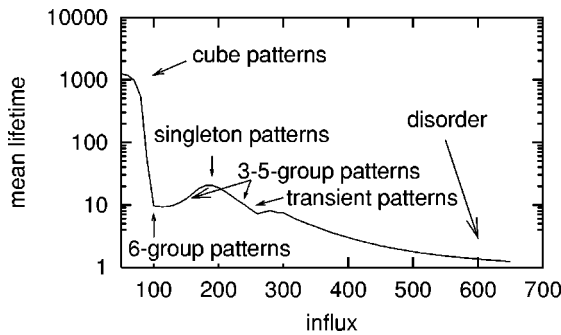

FIG. 20. Mean lifetime (log scale) versus influx for simulations on $G_{12}^{(2)}$ with $(t_1, t_u) = (1,10)$. Successively, the system forms cube patterns, multiple-group patterns, singleton patterns, and again multiple-group patterns. Then, patterns become transient and finally a randomness-driven regime is entered (see text).
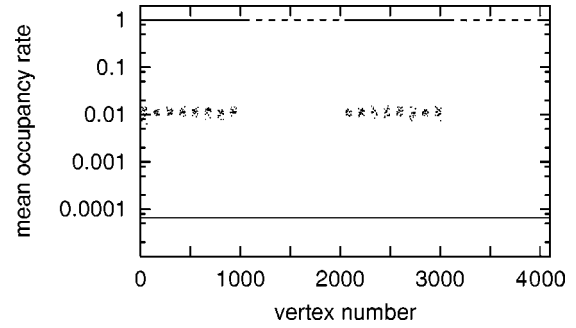

FIG. 21. Every vertex's mean occupancy obtained by a simulations on $G_{12}^{(2)}$ with $(t_1, t_u) = (1,10)$ and $I = 30$. Vertices are labeled by integers z corresponding to their respective bit chains. The relaxation time was $T_0 = 5000$; mean occupancies have been sampled over $T_1 - T_0 = 15\,000$ further time steps. An offset has been added to display the group S_L with the lowest mean occupancy $\langle s \rangle_{S_L} = 0$. The intermediate group S_M has mean occupancy $\langle s \rangle_{S_M} \approx 0.01$; the group with highest mean occupancy $\langle s \rangle_{S_H} \approx 1.0$.

lead to different numbers of groups and changing mean occupancy levels (depending on the time step when transitions occur) simulations performed with different initial conditions now always reproduce these six groups and their mean occupancies.

The interval of influxes $I \in [80,100]$ is characterized by transitions between both types of patterns in the course of which for higher influxes periods during which the six-group pattern is assumed more and more prevail. The change of the mean population averaged in both types of pattern is drastic: for $I = 90$ the cube pattern can sustain approximately $\langle n \rangle \approx 1024$ vertices while at the onset of their appearance six-group patterns can support a mean population of only about $\langle n \rangle \approx 600$ occupied sites. Comparing the mean occupancy levels of the six-group pattern with all previous pattern structures one remarks that, while groups of always empty sites are still present, groups of almost permanently occupied vertices are lacking. All groups have mean occupancy rates smaller than 0.7. This, and the relatively short lifetimes of vertices belonging to the groups S_4, S_5, and S_6 with high mean occupancy, speaks in favor of an interpretation as a "dynamic" pattern. Occupied vertices belonging to different groups "fluctuate" with different rates, while the interplay of
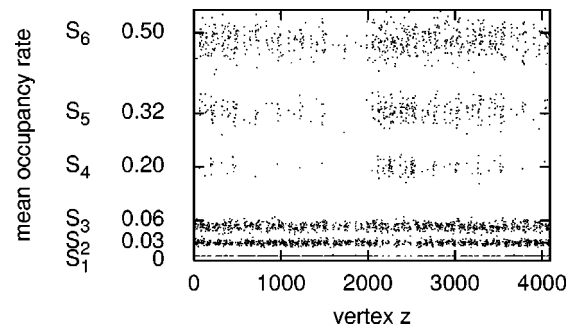

FIG. 22. Mean occupancy rates of vertices z derived from a simulation on $G_{12}^{(2)}$ with $(t_1, t_u) = (1,10)$ and $I = 100$. Six groups of vertices $S_1, \ldots, S_6 \subset G_{12}^{(2)}$ can be distinguished by their mean occupancy.

TABLE I. Data characterizing the six groups S_1, $\ldots$, S_6 obtained from simulations on $G_{12}^{(2)}$ with $(t_1, t_u) = (1,10)$ and $I = 100$. In 30 000 time steps vertices of S_1 have always belonged to the greatest subcluster of Γ_t, hence $\langle C_{\text{small}} \rangle$ could not be measured. Since they are immediately taken out after they get into the system, stable holes have a mean lifetime $\langle \tau \rangle = 0.0$. This means that their mean lifetime is shorter than the discretization of time.

Group S	$|S|$	$\langle C \rangle$	$\langle \tau \rangle$	$\langle r \rangle$	$\langle f_{\text{small}} \rangle$	$\langle C_{\text{small}} \rangle$	$\langle n \rangle$
S_1	1124	371.0	0.0	1.0	0.0		0.05
S_2	924	371.0	3.8	0.26	0.0	7.0	27.2
S_3	924	371.0	5.4	0.18	0.0	4.6	61.3
S_4	134	1.0	10.0	0.1	1.0	1.0	26.5
S_5	330	160	18.1	0.06	0.5	1.007	107.05
S_6	660	260	35.3	0.028	0.27	1.03	318.16

them secures that the distinct role of the groups is preserved. In the following the nature of this dynamic pattern will be elucidated in more detail.

Figure 22 and Table I give data characterizing these six groups: mean size of the cluster $\langle C \rangle$ on Γ_t that a vertex of a group belongs to, its mean lifetime $\langle \tau \rangle$, mean switch rate $\langle \overline{r} \rangle$, the mean frequency $\langle f_{\text{small}} \rangle$ of not belonging to the giant component, and the mean cluster size $\langle C_{\text{small}} \rangle$ of the small clusters if the vertex is not in the greatest component of Γ_t. On average, elements of S_1, S_2, and S_3 belong to 371 clusters on Γ_t, but are very seldom members of small clusters or singletons, have relatively short lifetimes and high switch rates. In contrast, elements of the groups of higher mean occupancy S_4, S_5, and S_6 typically have smaller mean cluster sizes, form more frequently small clusters, preferably singletons, and have long lifetimes. Mean lifetimes are increasing with increasing mean occupancy of the groups.

Exploring the interconnectedness and network structure of the groups $S_1, \ldots, S_6$ one obtains the following picture (cf. Fig. 23): The strongly interconnected groups S_2 and S_3 form a core of G to which—except S_4—all the other groups are attached. Excluding this core, each of the other groups consists of singletons. The largest set S_1 is a reservoir of stable holes and connects S_4 with the core. Thus, vertices of S_4 play a similar role as the previously mentioned isolated holes in the cube pattern: they receive their whole sustenance from the influx and have no permanent connections. While the group of second largest mean occupancy, S_5, has only links to the less populated part of the core, S_2; the most active vertices, elements of S_6, have connections with both parts of the core.

Consequently, apart from stimulation by random influx, elements of S_5 obtain stimulus from the core group S_3. Nevertheless, the stimulation is not optimal leading to a mean occupation of only 1/3 of S_5. The group S_6 receives stimulation from both core groups and so can support a higher population than S_5. Contrarily, since being strongly interconnected and connected to both the richly populated groups S_5 and S_6 most vertices of S_2 are suppressed. In the case of S_3, which does not connect to S_5, suppression is lower and thus a higher mean population can be sustained. The data shown
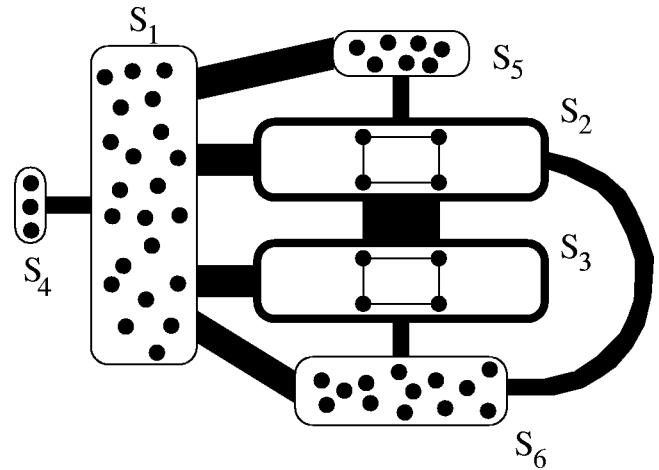

FIG. 23. Visualization of the network structure of the groups $S_1, \ldots, S_6$. The squares indicate many connections of vertices of a group among themselves, isolated circles in a group visualize that it consists of singletons. The thickness of the connecting lines gives a measure of the number of links connecting elements of different groups. Because of their importance for the existence of giant components in Γ_t, the core groups S_2 and S_3 are bounded by thick lines. Larger boxes correspond to larger groups.

in Table I are in qualitative agreement with this interpretation.

Figure 24 displays simulation data for the change of the relative occupations $s_i = 1/|S_i| \Sigma_{v \in S_i} \overline{s}(v)$, $i = 1, \ldots, 6$, of the six groups with increasing influx. Initially, all groups are clearly distinct, groups 4–6 have relatively low occupation and the mean populations of S_2 and S_3 are clearly above zero. As I grows while S_2 and S_3 lose population S_4, S_5, and S_6 become more populated, but at different rates. Thus, at $I \approx 150$ the groups S_4, S_5, and S_6 become united leading to the formation of a single set S_H of high mean occupancy vertices. A similar outcome is observed in the cases of S_1,
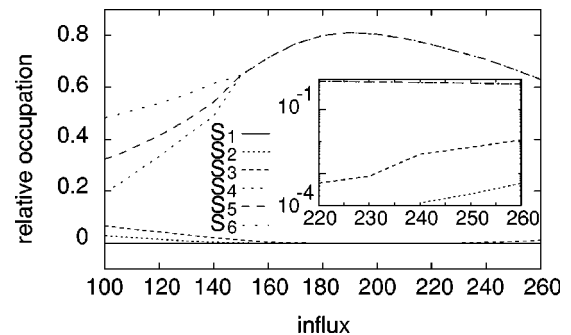

FIG. 24. Relative occupation $s_i = 1/|S_i| \Sigma_{v \in S_i} \overline{s}(v)$ of the six groups (labeled by their group number) for different influxes. For $I \approx 140$ groups S_1 and S_2 unite, for $I \approx 175$ S_3 joins them. At $I \approx 220$ S_3 again becomes separated, for $I \approx 240$ also S_2 disjoins from S_1. Similarly, S_4, S_5, and S_6 merge at $I \approx 150$. This leads to 5-group patterns ($I \in [140, 150]$), 4-group patterns ($I \in [150, 175]$ and $I \in [240, 260]$), singleton patterns ($I \in [175, 220]$), and a 3-group pattern ($I \in [220, 240]$). For $I > 260$ transitions between isomorphic configurations set in.

S_2, and S_3. For $I \approx 140$ group S_2 joins S_1 and becomes indistinctive from S_3 at $I \approx 175$, leading thus to a single low occupancy group S_L. During this process the overall mean population of Γ_t, $\langle n \rangle$, is growing. Consequently, for $I \in [175, 220]$ again a 2-group pattern of 1124 high-mean-occupancy and 2972 low-mean-occupancy vertices appears, consisting now entirely of long-living singletons "sustained by the influx." Transition patterns before this pattern appears are 5- and 4-group patterns, after it grew unstable 3-group patterns are forming.

As I is further increased the influx that heretofore guaranteed the sustenance of S_5 and S_6 gradually causes overstimulation. Thus, the mean populations of S_5 and S_6 are shrinking, causing, in turn, less overstimulation of the core. So, again a small population can persist in S_2 and S_3. Altogether, for further increased influx the different groups disentangle, leading to a revival of the multigroup patterns.

From $I \approx 260$, on these dynamic multiple group patterns become unstable and rearrangements between different (isomorphic) configurations set in. Analogous to the scenario discussed in Sec. V B disordered periods dominate more and more and finally lead to disorder.

Interestingly, the group structure allows some insight into the actual cluster structure of Γ_t at an arbitrary time step. Obviously, giant and greater clusters on Γ_t can only emerge as long as the core is populated. As the mean population of S_2 does not suffice to form a giant component within S_2, S_3 functions as the "glue" of giant clusters on Γ_t. Elements of the "backbone" of the giant cluster preferably come from S_2 and S_3. As the population of S_2 decreases vertices of S_5 increasingly become detached from the core and tend to form small clusters and singletons.

A great component, however, is still retained by elements of S_6 and S_2 bound together by S_3. As the population of S_2 also sinks below a certain threshold, greater components of Γ_t become starlike, their hubs being in S_3. Finally clusters different from singletons completely vanish, resulting in purely influx sustained patterns of singletons.

VII. PATTERNS FOR $t_l > 1$

For completeness in this section stationary patterns appearing for lower thresholds $t_l > 1$ will be sketched briefly.

Figure 25 displays data for the mean occupancy rates of every vertex gathered from a simulation on $G_{11}^{(1)}$ with $(t_l, t_u) = (3, 10)$. One realizes two relatively broad bands of mean occupancy rates. Investigating the structures of $S_H = S(0.5)$ and $S_L = G \setminus S_H$ reveals that, analogously to the $t_l \leq 1$ situation both high- and low-mean-occupancy groups completely decay into 2-clusters. Now, however, such 2-cluster patterns are only existing with mean occupancy rates $\langle s \rangle_{S_H}$ significantly smaller than 1 and $\langle s \rangle_{S_L}$ far above zero. Thus, since a "frozen" 2-clustered state (see Sec. III) cannot subsist for $t_l > 1$, a fluctuating 2-cluster pattern is formed. At every single time step only a part of the high-mean occupancy vertices is occupied. As a consequence, not all holes are stable. A part of the holes can become occupied, thus giving the necessary stimulation to the vertices of S_H
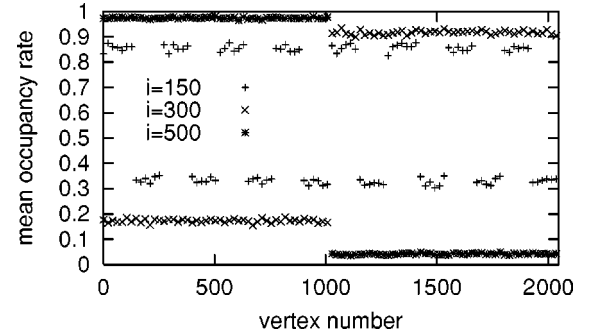

FIG. 25. The mean occupancy rate of every vertex from simulations on $G_{11}^{(1)}$ with $(t_1, t_u) = (3, 10)$ and influxes $I = 150$, 300, and 500. For low influx both the high-mean-occupancy group and low-mean-occupancy group are considerably apart from their extreme values 1 and 0. As I grows, S_L becomes less occupied and vertices of S_H evolve to an almost permanent presence. Thus, increasing I further the high mean occupancy set loses stimulation and the pattern becomes unstable.

which are present. On average, whereas elements of S_L have high occupied neighbor degrees (and are on the verge of being overstimulated), elements of S_H have low occupied neighbor degrees (and are threatened by understimulation). On the whole, however, vertices occupying such holes tend to get removed with higher probability. One can imagine this situation as a pattern of long-living occupied 2-clusters flown round by short-living 1- and 2-clusters, living just for their stimulation.

Considering this situation as evolved from an ideal 2-cluster pattern $B_{(s_0, P)}$ one understands that it can only survive for an intermediate range of influxes. On the one hand, if the influx is too low, not enough occupied sites are driven out by overstimulation that holes could lose stability. Thus, the sites occupied in the ideal pattern B did not receive the necessary stimulation and the pattern was unstable. On the other hand, too high influx causes more and more of the frequently occupied vertices to be almost permanently occupied. This but leads to many stable holes. So, for higher influxes an abrupt transition to disorder occurs. The intermediate behavior (transitions between isomorphic configurations) is lacking in this case.

VIII. CONCLUSIONS

To conclude, we have presented a probabilistic model for a local-rule governed evolution of occupied and empty sites on regular graphs G. Aiming chiefly at a description of INW's in the immune system we studied two types of base graphs $G^{(1)}$ and $G^{(2)}$ created by describing idiotypes by bit strings and their functional interactions by "matching rules." In contrast to most modeling approaches to idiotypic networks [5], the model abstains from all details of the dynamics of the real-life interactions of cells, but aims at understanding principal mechanisms of network formation.

On $G^{(1)}$ and $G^{(2)}$ the dynamics generated by the window algorithm leads to organized network structures, which consist of functionally different subsets, distinguished, e.g., by their mean occupancy. On both types of base graphs for in-

fluxes I small compared to the system size, a multitude of such network patterns has been found. We developed a notion of pattern stability and classified them as metastable. For larger influxes one type of pattern prevails. In the case of the one-mismatch graphs $G^{(1)}$ patterns for intermediate influx always consist of an arrangement of 2-clusters of holes and occupied vertices. We have given a classification of these patterns and have described fluctuations around an ideal pattern structure by a statistical approach via defects. For $I > I_c$ these 2-clustered patterns become unstable, and the system starts oscillating between periods during which a pattern structure prevails and periods of disorder. Finally, increasing I further, the dynamics is marked by randomness and extremely short lifetimes. We elucidated the nature of these transitions.

These 2-clusters are nothing but the idiotype–anti-idiotype pairs that have been proposed as one mechanism for the preservation of memory of previously encountered antigen. (The anti-idiotype represents the internal image of the antigen [21,36].) Their arrangement in a coherent pattern, however, leads to an overall memory capacity of the network that increases only logarithmically with the system size. This is clearly insufficient for a real immune system. The parameter range where the coherent 2-cluster patterns emerge can therefore not be the working regime of a healthy immune system.

It is worthwhile to note that in this regime (and in all regimes allowing for memory on $G^{(2)}$) the network connectivity decreases with growing simulation time, i.e., with growing age. This is in accord with experimental observations and was also found in other modeling approaches [5]. It suggests that the networks' gradually losing links is an essence of the limited range of allowed occupied neighbor degrees and hence of crosslinking.

On the more densely wired graphs $G^{(2)}$ cube patterns have been found for an intermediate range of influxes. Increasing I beyond a threshold, the system then settles into dynamic "multiple-group" patterns. In this regime, several subsets S_j of the base graph $G^{(2)}$ can be distinguished according to their mean occupancy. Vertices of these subsets also differ in the structure of the cluster on Γ_t, which they typically belong to. Two of these subsets form a strongly interconnected core on Γ_t, to which vertices of the other groups are bound with different strengths. Each of the other subsets consists only of singletons and links to the core and some of the other groups. The core groups have been found to be always rarely populated, the major fraction of the population being typically contained in two of the other groups.

The structure encountered in this parameter regime is in very good agreement with general ideas about the topology of INW's [21,27,37–39]. It exhibits a structured core that could correspond to a central part generally believed to exist in INW's. Furthermore, richly populated noncore groups are in good agreement with the notion of a peripheral part of INW's. Long lifetimes of vertices belonging to these groups are in accord with the idea that the peripheral part of the network is responsible for the preservation of idiotypic memory.

The issue about the in detail working of idiotypic memory

is still much disputed. Apart from the "internal image hypothesis" several mechnisms are currently known [40–43]. One of these bases on certain cells (folicular dendritic cells) that occasionally exhibit parts of antigen, which is deemed enough to sufficiently stimulate the complementary idiotype—allowing in this way idiotypic memory in a single antigen-specific clone.

Derived from our model, a mechanism for idiotypic memory seems possible: Memory could be retained in a single antigen-specific clone that is not preferably stimulated, but occasionally receives stimulation from the central part of the network and from new complementary idiotypes from the bone marrow which serves as a background stimulus. This mechanism could collaborate with antigen presentation by follicular dendritic cells.

Two further issues that follow from the multigroup structure of networks in our model seem worthwhile to note.

First, during its evolution the system generates a group S_1 of always suppressed idiotypes. Although the dynamics of antigens differs from that of idiotypes, the existence of such a group implies that there should be a set of antigens against which an individual is immune, without ever having been immunized against. More speculatively, one could identify the set S_1 with a "mirror image of the molecular self." Following this interpretation, antibodies belonging to S_1 are autoreactive, but are almost always suppressed by the remainder of the network. The actual location of this set is determined by encounters with other antigens and, chiefly, by the fortuitous history of the deployment of bone marrow influx during early life.

As a second fact, while the number of autoantibodies increases [44], the bone marrow production is known to decrease with growing age [42]. Here, additional to a decline in connectivity till stationarity is reached, our model suggests another structural alteration of the network. Assuming for young individuals a working point of INW's that is above the parameter regime of single-clone patterns, a decreased bone marrow production leads to smaller cores and an increasing periphery, i.e., an accumulation of memory and loss of plasticity.

Summarizing our main result, taking into account different levels of coarse graining of reaction affinities between idiotypes—as represented by the base graphs $G_d^{(1)}$ and $G_d^{(2)}$—leads to two different regimes of steady-state behaviors: (i) rigid "coherent" configurations on $G^{(1)}$ and (ii) dynamic patterns on $G^{(2)}$ which are increasingly dominated by 1-clones. We conjecture that generally isolated clones are a consequence of a high connectivity of the network and high interaction strength between idiotypes. It is suggestive that the bone marrow influx is a driving mechanism for shaping the structure of INW's, which together with the interaction strength of idiotypes, determines the working point of an INW.

[1] H. Jeong, B. Tombor, R. Albert, Z.N. Oltvai, and A.-L. Barabási, Nature (London) **407**, 651 (2000).

[2] D.A. Fell and A. Wagner, Nat. Biotechnol. **18**, 1121 (2000).

[3] J.M. Montoya and R.V. Solé, J. Theor. Biol. **214**, 405 (2002).

[4] F. Liljeros, C.R. Edling, L.A. Nunes Amaral, H.E. Stanley, and Y. Aberg, Nature (London) **411**, 907 (2001).

[5] A.S. Perelson and G. Weisbuch, Rev. Mod. Phys. **69**, 1219 (1997).

[6] S.H. Strogatz, Nature (London) **410**, 268 (2001).

[7] P. Erdös and A. Rényi, Publ. Math. **6**, 290 (1959).

[8] B. Bollobás, *Random Graphs* (Academic Press, London, 1985).

[9] M.E.J. Newman, S.H. Strogatz, and D.J. Watts, Phys. Rev. E. **64**, 026118 (2001).

[10] D. Stauffer and A. Aharony, *Perkolationstheorie: eine Einführung* (VCH, Weinheim, 1995).

[11] A.-L. Barabási and R. Albert, Science **286**, 509 (1999).

[12] G.B. West, J.H. Brown, and B.J. Enquist, Science **284**, 1677 (1999).

[13] N. Mathias and V. Gopal, Phys. Rev. E, **63**, 021117 (2001).

[14] R. Ferreri Cancho and R.V. Solé, www.santafe.edu/sfi/publications/wpabstract/200111068

[15] S. Jain and S. Krishna, Phys. Rev. E, **65**, 026103 (2002).

[16] S. Jain and S. Krishna, Proc. Natl. Acad. Sci. U.S.A. **99**, 2055 (2002).

[17] D.S. Callaway, J.E. Hopcroft, J.M. Kleinberg, M.E.J. Newman, and S.H. Strogatz, Phys. Rev. E. **64**, 041902 (2001).

[18] R. Albert and A.-L. Barabási, Rev. Mod. Phys. **74**, 47 (2002).

[19] D.J. Watts, *Small Worlds* (Princeton University Press, Princeton, 1999).

[20] S.N. Dorogovtsev and J.F.F. Mendes, Adv. Phys. **51**, 1079 (2002).

[21] N.K. Jerne, Ann. Immunol. (Inst. Pasteur) C **125**, 373 (1974).

[22] M. Shannon and R. Mehr, J. Immunol. **162**, 3950 (1999).

[23] I.CM. MacLennan, Curr. Opin. Immunol. **10**, 220 (1998).

[24] E.R. Berlekamp, J.H. Conway, and R.K. Guy, *Winning Ways for Your Mathematical Plays* (Academic Press, London, 1982), Vol. 2.

[25] P. Bak, K. Chen, and M. Creutz, Nature (London) **342**, 780 (1989).

[26] F.J. Varela and A. Coutinho, Immunol. Today **5**, 159 (1991).

[27] B. Sulzer, J.L. van Hemmen, and U. Behn, Bull. Math. Biol. **56**, 1009 (1994).

[28] J.D. Farmer, N.H. Packard, and A.S. Perelson, Physica D **22**, 187 (1986).

[29] Yu. M. Svirezhev and D.O. Logofet, *Stability of Biological Communities* (MIR, Moscow, 1983).

[30] For $t_1 = 0$ the window algorithm can be reformulated from a holes' point of view. Let $\partial_0 v = \kappa - \partial v$ denote the number of empty sites adjacent to a vertex v. According to step (2) of the window algorithm an occupied vertex is taken out if $\partial v > t_u$. The idea of stable holes implies that holes h can only be taken out if $\partial h = \kappa - \partial_0 h < t_u + 1$. Thus, holes h can only be removed if $\partial_0 h > t_u^{hole} = \kappa - t_u + 1$, which is—considering the time scales at which holes are probed frequently enough—the same rule as for occupied vertices.

[31] There are $\binom{I}{j}$ variants to choose j out of I vertices that are to be placed in the neighborhood of a specified occupied vertex. Then, since it has a 2-cluster mate, $\binom{\kappa-1}{j}$ choices to distribute these j vertices in this vertex's 1 neighborhood remain. The last factor gives the number of ways how the other $I - j$ vertices can be distributed on the remaining $N - (\kappa - 1)$ holes of the pattern.

[32] M. Brede and U. Behn, Phys. Rev. E **64**, 011908 (2001).

[33] This can be understood as a result of two competing mechanisms. On the one hand, higher t_u demands less vertices to be taken out in order to make a hole unstable. On the other hand, however, the effort to remove a vertex grows with t_u. It can be easily verified that the second tendency outweighs the first one.

[34] C.A. Bona, Proc. Soc. Exp. Biol. Med. **213**, 32 (1998).

[35] P.J. Ruiz *et al.*, Nat. Med. **4**, 710 (1998).

[36] U. Behn, J.L. van Hemmen, and B. Sulzer, J. Theor. Biol. **165**, 1 (1993).

[37] A. Coutinho, Immunol. Rev. **110**, 63 (1989).

[38] I.R. Cohen, Immunol. Today **12**, 490 (1992).

[39] F.J. Varela and A. Coutinho, Immunol. Today **5**, 159 (1991).

[40] R.M. Zinkernagel *et al.*, Annu. Rev. Immunol. **14**, 333 (1996).

[41] J. Sprent, Curr. Opin. Immunol. **9**, 371 (1997).

[42] A.A. Freitas and B. Rocha, Annu. Rev. Immunol. **18**, 83 (2000).

[43] R. Nayak, S. Mitra-Kaushik, and M.S. Shaila, Immunology **102**, 387 (2000).

[44] R. Attanasio *et al.*, Clin. Exp. Immunol. **123**, 361 (2001).